AD-756 498

AN INVESTIGATION OF AN UPPER STAGE ROCKET PLANE WITH EXTERNAL-BURNING THRUST AUGMENTATION

E. E. Callens, et al

Arnold Engineering Development Center
Arnold Air Force Station, Tennessee

February 1973

DISTRIBUTED BY:

NTIS

National Technical Information Service
U. S. DEPARTMENT OF COMMERCE
5285 Port Royal Road, Springfield Va. 22151

AEDC-TR-72-181

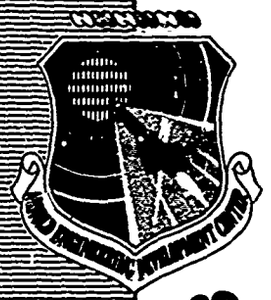

AD756498

AN INVESTIGATION OF AN UPPER STAGE ROCKET PLANE WITH EXTERNAL-BURNING THRUST AUGMENTATION

E. E. Callens, J. T. Miller, and J. L. Potter

ARO, Inc.

February 1973

DDC
RECEIVED
MAR 6 1973
E

Approved for public release; distribution unlimited.

Reproduced by
NATIONAL TECHNICAL
INFORMATION SERVICE
U S Department of Commerce
Springfield VA 22151

VON KÁRMÁN GAS DYNAMICS FACILITY
ARNOLD ENGINEERING DEVELOPMENT CENTER
AIR FORCE SYSTEMS COMMAND
ARNOLD AIR FORCE STATION, TENNESSEE

R

NOTICES

When U. S. Government drawings specifications, or other data are used for any purpose other than a definitely related Government procurement operation, the Government thereby incurs no responsibility nor any obligation whatsoever, and the fact that the Government may have formulated, furnished, or in any way supplied the said drawings, specifications, or other data, is not to be regarded by implication or otherwise, or in any manner licensing the holder or any other person or corporation, or conveying any rights or permission to manufacture, use, or sell any patented invention that may in any way be related thereto.

Qualified users may obtain copies of this report from the Defense Documentation Center.

References to named commercial products in this report are not to be considered in any sense as an endorsement of the product by the United States Air Force or the Government.

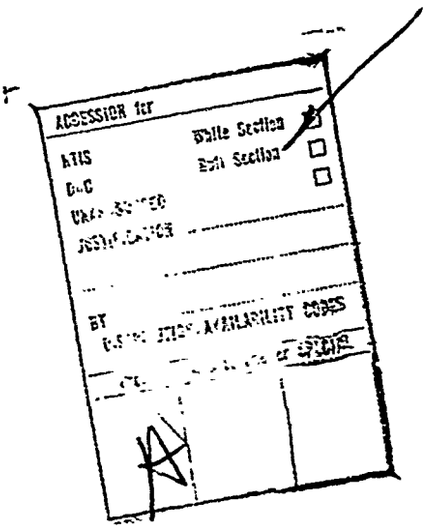

UNCLASSIFIED

Security Classification

DOCUMENT CONTROL DATA - R & D

(Security classification of title, body of abstract and indexing annotation must be entered when the overall report is classified)

1 ORIGINATING ACTIVITY (Corporate author) Arnold Engineering Development Center Arnold Air Force Station, Tennessee 37389	2a. REPORT SECURITY CLASSIFICATION UNCLASSIFIED 2b. GROUP N/A

3 REPORT TITLE

AN INVESTIGATION OF AN UPPER STAGE ROCKET PLANE WITH EXTERNAL-BURNING THRUST AUGMENTATION

4 DESCRIPTIVE NOTES (Type of report and inclusive dates)

Final Report -

5 AUTHOR(S) (First name, middle initial, last name)

E. E. Callens, J. T. Miller, and J. L. Potter, ARO, Inc.

6 REPORT DATE February 1973	7a. TOTAL NO. OF PAGES 69 71	7b. NO. OF REFS 67
8a. CONTRACT OR GRANT NO b. PROJECT NO. c. Program Element 65802F d.	9a. ORIGINATOR'S REPORT NUMBER(S) AEDC-TR-72-181 9b. OTHER REPORT NO(S) (Any other numbers that may be assigned this report) ARO-VKF-TR-72-94	

10 DISTRIBUTION STATEMENT

Approved for public release; distribution unlimited.

11 SUPPLEMENTARY NOTES Available in DDC	12 SPONSORING MILITARY ACTIVITY Arnold Engineering Development Center, Air Force Systems Command, Arnold AF Station, TN 37389

13 ABSTRACT

Some fundamental aspects of a regeneratively cooled, upper stage rocket plane with external-burning thrust augmentation are investigated analytically. Cases condidered are (1) only the ejected coolant is burned externally and (2) all of the thrust required for sustained cruise is provided by external burning. One conclusion is that external-burning configurations offer an apparent advantage over internal propulsion systems in that the total vehicle cooling requirement for high-speed operation is much less for the external-burning regeneratively cooled configuration. Also, the fuel required for propulsion by an external-burning configuration greatly exceeds the fuel required for cooling. Two important consequences are (1) the cooling efficiency of the fuel may be a secondary consideration in the choice of fuel, with the heating value, specific weight, and volumetric requirements becoming the primary criteria and (2) since the excess cooling capability is available, the possibility remains that vehicle configurations which require additional cooling might be used without undue penalty. Configurations include those with multiple compression shocks for improved compression efficiency, waveriders, and even internal- burning configurations. In terms of propulsion efficiency, i.e., specific impulse, external burning offers an advantage over pure rocket propulsion up to about Mach 20. Although this appears to be a large advantage, the very small thrusts required at high velocities and high altitudes tend to discount this advantage.

DD FORM 1 NOV 65 1473

Security Classification

14. KEY WORDS	LINK A		LINK B		LINK C	
	ROLE	WT	ROLE	WT	ROLE	WT
aerospaceplanes						
external combustion						
cooling						
propulsion systems						
hypersonic flight						

FOREWORD

The research reported herein was conducted by Headquarters, Arnold Engineering Development Center (AEDC), Air Force Systems Command (AFSC), Arnold Air Force Station, Tennessee, under Program Element 65802F.

Research results were obtained by ARO, Inc. (a subsidiary of Sverdrup & Parcel and Associates, Inc.), contract operator of AEDC. The ARO Project Numbers were BE2152 and BE2256, and the manuscript was submitted for publication on June 20, 1972.

This technical report has been reviewed and is approved

ROBERT O. DIETZ
Director of Technology

ABSTRACT

Some fundamental aspects of a regeneratively cooled, upper stage rocket plane with external-burning thrust augmentation are investigated by analyzing simplified models. Cases considered are (1) only the ejected coolant is burned externally and (2) all of the thrust required for sustained cruise is provided by external burning. Several conclusions can be drawn on the basis of this study. One conclusion is that the fuel required for propulsion by an external-burning configuration may exceed the fuel required for cooling the windward aerodynamic surfaces. This has two important consequences. First, the cooling efficiency of the fuel may be a secondary consideration in the choice of fuel, with the heating value, specific weight, and volumetric requirements becoming the primary criteria. Secondly, since an excess cooling capability is available, the possibility remains that vehicle configurations which require additional cooling might be used without undue penalty. Possible configurations include those with multiple compression shocks for improved compression efficiency and waveriders. In terms of propulsion efficiency, i.e., specific impulse, scramjets with internal or external burning offer an advantage over pure rocket propulsion up to about Mach 20. Although this appears to be a large advantage, the very small thrusts required at high velocities and high altitudes tend to discount this advantage, especially when the technical difficulties of developing an operational external combustor are weighed against the simplicity of operational, throttlable rocket engines.

CONTENTS

ILLUSTRATIONS

Preceding page blank

NOMENCLATURE

A	Area
C	Temperature-viscosity factor, $\mu = CT$
C_D	Drag coefficient
C_F	Average friction drag coefficient
C_L	Lift coefficient
C_p	Specific heat or pressure coefficient
D	Drag
F'	Ratio of blown mass flux to free-stream mass flux
F_t	Thrust
g	Acceleration of gravity
H	Enthalpy
h	Altitude
h_{H_2}	Heating value of hydrogen
h^*	Reference value of enthalpy
L	Lift
ℓ	Length
M	Mach number
$\dot{m}$	Mass flow rate
Pr	Prandtl number
p	Pressure
$\dot{q}$	Heat flux
$\dot{q}_w$	Convective heating rate
R	Gas constant
Re	Reynolds number
S	Reference area
T	Temperature
t	Thickness
U	Velocity

U_e	Exhaust velocity
$\bar{V}_\infty$	Viscous interaction parameter
W	Weight
$\dot{W}_{H_2}$	Hydrogen fuel flow rate
x	Distance from leading edge
x_1	Extent of cooled surface
Z_o	Radius of earth
α	Angle of attack
β	Flow turning angle at knee
γ	Ratio of specific heats
δ	Initial wedge angle
ϵ	Emissivity
θ	Bow shock wave inclination angle
μ	Viscosity
μ_1	Prandtl-Meyer flow angle
ρ	Density
σ	Stephan-Boltzmann constant or shock wave angle
$\dot{\omega}_{H_2}$	Flow rate of hydrogen required for cooling

SUBSCRIPTS

1	Denotes condition behind bow shock
2	Denotes condition at knee
3	Denotes exit conditions
av	Available
E	Environment
i	Inlet
inv	Inviscid
ℓ	Reference length
max	Maximum
p	Pressure

R	Radiation
req	Required
ST	Storage capacity
s	Denotes condition behind shock wave
w	Wall
o	Stagnation
∞	Free stream
ȯ	Local edge of boundary-layer condition

SUPERSCRIPT

*	Denotes reference value

SECTION I
INTRODUCTION

In the early 1950's, there was considerable interest in the United States in the development of an "aerospaceplane" which was envisaged as a completely reusable, maneuverable hypersonic aircraft capable of reaching orbital conditions. The vehicle was to utilize an airbreathing propulsion system and be able to take off and land horizontally. Although the concept was generally regarded as involving no impossibilities or improbabilities, its development was viewed as pushing the very fringes of technology. Additionally, the nonreusable but more fully developed and reliable multistage rocket could satisfy potential mission requirements for some time to come. As a result, the aerospaceplane became a concept awaiting an advancing technology.

In the intervening years, there has been advancement in the technology directly applicable to this concept. For example, studies have been made of the propulsive lifting body which combines the advantages of the hypersonic waverider with supersonic external combustion, exploiting the strong-shock-wave flow which is characteristic of high-speed flight. Also, advances in regenerative-cooling technology have rendered the external aerodynamic heating and internal propulsive heating problems tenable. In view of these and other technological developments, a renewed interest in the potential performance of an aerospaceplane is justified.

This report focuses on the fundamental aerodynamics of a simple propulsive lifting body considered to be the upper stage of a two-stage vehicle. The propulsion system for the upper stage consists of rocket engines and external combustion. This "rocket plane" is designed to cruise anywhere between 100,000 ft and orbit at Mach numbers above 6. The external surfaces are cooled by a combination of surface radiation and supplemental regenerative cooling using hydrogen. The equilibrium surface temperature is maintained at or below a maximum of 2100°F (1400°K), and the heated hydrogen is dumped into the external stream. This hydrogen can be utilized as fuel in the external combustion process.

The function of the external combustion engine in augmenting the thrust of the rocket engine through burning of the ejected coolant is investigated. Additionally, the condition wherein external burning provides the entire thrust required for sustained cruise is studied.

This study is intended only to single out some fundamental problems or constraints of hypersonic flight. Therefore, simple approximate

analysis is chosen over more thorough methods which might improve precision without changing any of the conclusions.

SECTION II
BACKGROUND

2.1 FLIGHT DOMAIN CONSTRAINTS

Sustained cruise at a particular altitude requires that the sum of the aerodynamic lift and the centrifugal force, attributable to the curvature of the flight path, be equal to the weight of the vehicle. Thus,

$$W = (1/2)C_L \rho_\infty U_\infty{}^2 S + (W/g)\frac{U_\infty{}^2}{(Z_o + h)} \tag{1}$$

or

$$1 = \left(\frac{C_L S}{W}\right)\frac{\rho_\infty U_\infty{}^2}{2} + \frac{U_\infty{}^2}{g(Z_o + h)} \tag{2}$$

where W/S is the wing loading and C_L is the lift coefficient. The maximum value of $(C_L S/W)$ is a constraint, which is imposed by the specific vehicle design and which determines the maximum altitude at which flight at a particular velocity can be sustained. Therefore, lines of constant $(C_L S/W)$ in altitude-velocity space represent maximum altitudes which can be achieved by a particular vehicle at a particular velocity.

Lines of constant $(C_L S/W)$ have been computed and plotted in the altitude-velocity plane in Fig. 1. Values of $(C_L S/W)$ have been chosen by imposing the requirement that the vehicle be capable of flight at 100,000 ft with a dynamic pressure of 50, 100, 200, 500, 1000, or 2000 lb/ft^2.

If a vehicle is designed to achieve a certain maximum value of $(C_L S/W)$, sustained operation at substantially lesser values is probably not possible. For example, if the design point is cruise at a dynamic pressure 100 lb/ft^2, flight at a dynamic pressure of 200 lb/ft^2 requires a more rigid structure, which means more structural weight, which, in turn, lowers the maximum value of $(C_L S/W)$. Therefore, the appreciable deviation of a vehicle from a line of constant $(C_L S/W)$ in the velocity-altitude plane is unlikely.

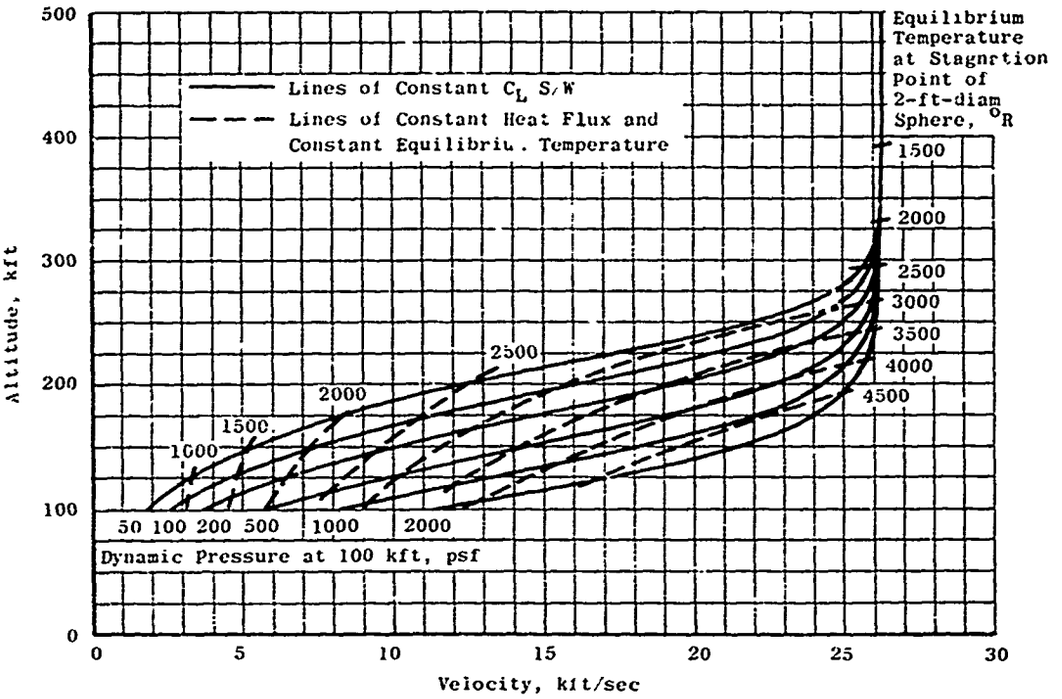

Fig. 1 Flight Corridor Constraints Based on Aerodynamic Lift Requirement

Aerodynamic heating considerations introduce additional weight penalties. For high-speed flight, the interior of the vehicle must be insulated from the skin in order to maintain interior temperatures within allowable levels. This insulation and supporting structure make a contribution to the vehicle weight and thus have a detrimental effect on the $(C_L S/W)_{max}$ obtainable.

As the aerodynamic heating is further increased, some portions of the vehicle leading edges must have special heat shielding. This adds a significant weight penalty, further restricting the $(C_L S/W)_{max}$. Thus, a high-velocity cruise capability at low altitudes is not readily compatible with flight at high altitudes.

A measure of the thermal severity of the environment can be obtained by calculating the equilibrium temperature of a surface exposed to the environment. At equilibrium, the convective heating load can be equated to the heat loss rate by radiation from the surface. For these specific calculations, the convective heat rate used is appropriate for laminar heating at the stagnation point of a 2-ft-diam sphere. Figure 2 shows these equilibrium temperatures appropriate to the flight paths shown in Fig. 1. Constant temperature lines then represent lines of constant heating load. These lines are shown in Fig. 1 and should be interpreted as measures of the severity of the thermal environment, rather than absolute temperature limits.

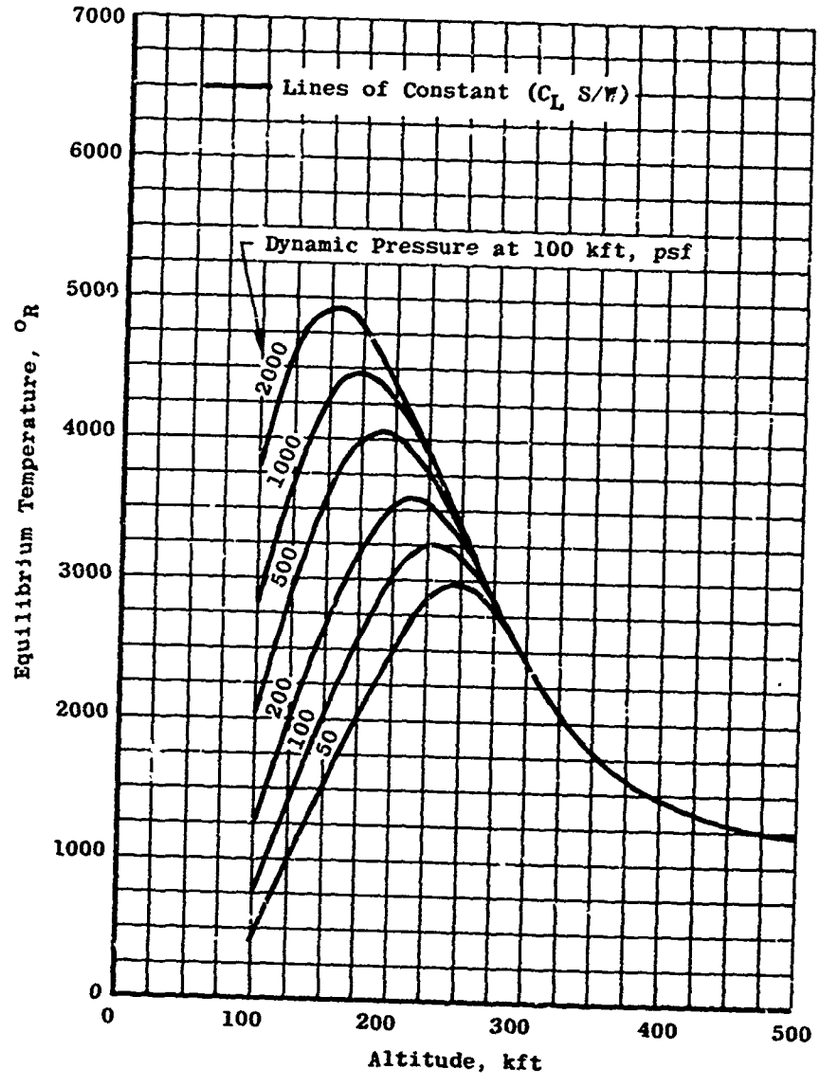

Fig. 2 Equilibrium Temperature at Stagnation Point of 2-ft-Diam Sphere

A second constraint is that sufficient thrust be available to balance the aerodynamic drag. Thus,

$$F_{t,req} = D = (1/2)C_D\rho_\infty U_\infty{}^2 S \tag{3}$$

The drag coefficient, C_D, and the area, S, are fixed by vehicle configuration and operating conditions. When C_DS is constant, the thrust requirement varies as dynamic pressure, so that lines of constant dynamic pressure in the altitude-velocity plane approximate lines of constant thrust for given C_DS.

Lines of constant dynamic pressure (thrust requirement) are shown in Fig. 3, along with lines of constant ($C_L S/W$). The dynamic pressure range used is the same as for Fig. 1. As can be seen in Fig. 3, variations toward higher altitudes and velocities along a constant ($C_L S/W$) curve result in a decreasing thrust requirement, and conversely, flight along a constant drag curve can result in excess lift over that required to sustain the cruise altitude.

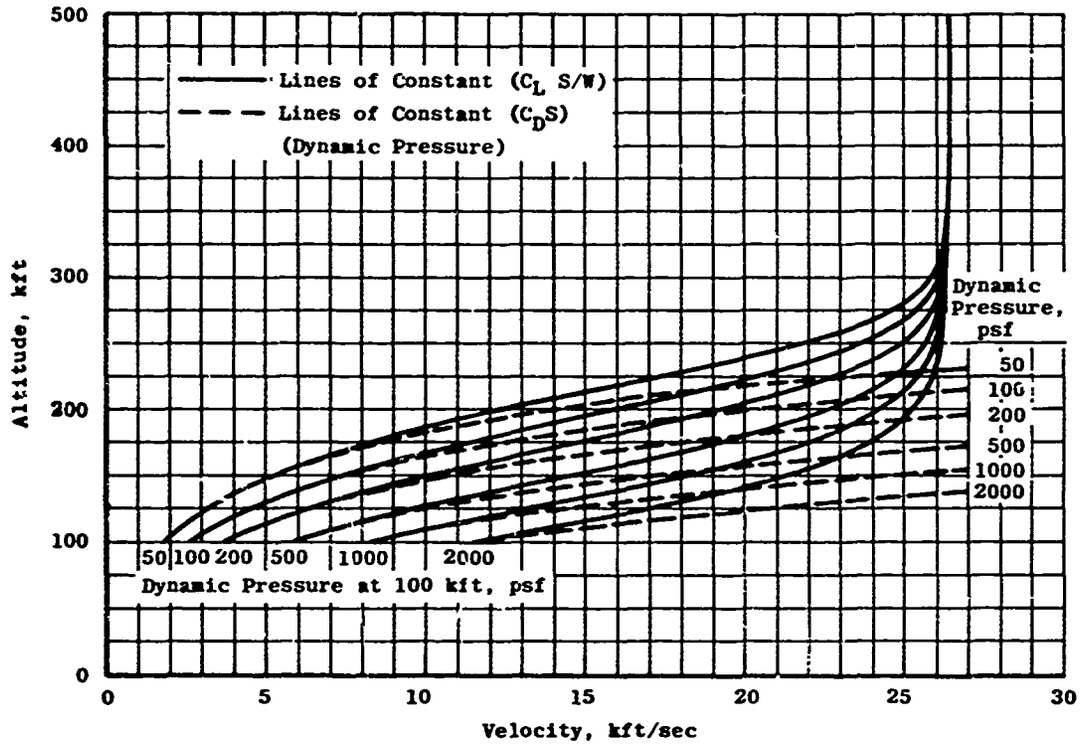

Fig. 3 Flight Corridor Constraints Based on Thrust Requirements

Another general problem area is the variation with altitude and velocity of the thrust available from an air-breathing engine. An air-breathing engine produces thrust by ingesting air, heating the air, converting the thermal energy to kinetic energy, and finally expelling the air at an exit velocity which is higher than the entrance velocity. From momentum considerations, the thrust, F_t, can be expressed as

$$F_t = A\rho_\infty U_\infty (U_3 - U_\infty) \tag{4}$$

where A is the inlet area, ρ_∞ is the ambient density, U_∞ is the free-stream velocity, and U_3 is the exit velocity. This expression neglects the contributions attributable to the difference between inlet and exit pressures and mass addition of fuel. Equation (4) shows that the exit

velocity, U_3, should be as large as possible. If hydrogen is used as a fuel, a maximum temperature in the propulsion system should be below 7200°R to prevent dissociation of the combustion products and attendant inefficiencies (Ref. 1, 1968). This assumed temperature limitation is quite optimistic from a materials standpoint. The maximum attainable exit velocity is governed by the maximum temperature, through the energy equation. Assuming the most efficient conversion of thermal energy to kinetic energy, the relationship between maximum temperature and exit velocity is

$$C_p T_i + C_p \Delta T + U_i^2/2 = U_3^2/2 \tag{5}$$

where T_i is the inlet temperature, ΔT is the temperature increase in the engine, and U_i is the inlet velocity (hereafter assumed equal to U_∞).

In a subsonic combustion process, the entering air is decelerated to subsonic velocities before combustion, with an attendant rise in air temperature. The maximum temperature is then given by

$$C_p T_{max} = C_p T_i + C_p \Delta T + U_\infty^2/2 \tag{6}$$

Therefore, combining Eqs. (5) and (6) with C_p taken to be 6007.4 ft^2/sec^2 °R and T_{max} = 7200°R, the maximum exit velocity is

$$U_3 = \sqrt{2 C_p T_{max}} \approx 9300 \text{ ft/sec} \tag{7}$$

From Eq. (4), it can be seen that no thrust can be obtained from a subsonic combustion process with flight velocities equal to or greater than 9300 ft/sec, the maximum exit velocity possible using hydrogen fuel.

In order to examine the variation of thrust from a particular engine with changes in velocity and altitude, it has been assumed that the engine is designed to provide sufficient thrust for level flight at 100,000-ft altitude and dynamic pressures of 50, 100, and 200 lb/ft^2. Lines of constant thrust have been plotted in Fig. 4 for these engines with the assumption that the inlet area is fixed. This plot shows that the thrust of a particular engine has a maximum at a flight velocity of $U_3/2$. Therefore, engines with subsonic combustion processes look unattractive for flight velocities greater than about 5000 ft/sec.

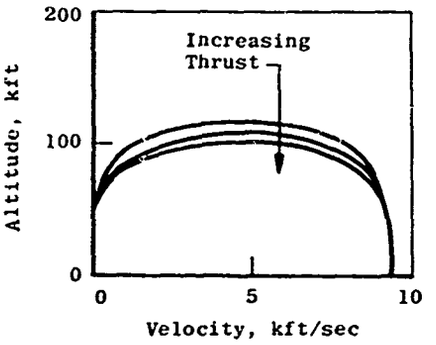

Fig. 4 Representative Altitude-Velocity Relationship for Constant Thrust Available from a Particular Engine—Subsonic Combustion (Eqs. (4) and (7))

In the case of supersonic combustion, the maximum temperature limitation (analogous to Eq. (6)) is applicable to the sum of the inlet temperature plus the temperature rise, since the flow is not appreciably decelerated. Then

$$C_p T_{max} = C_p T_i + C_p \Delta T \tag{8}$$

Combining Eqs. (5) and (8), the maximum exit velocity is

$$U_3 = \sqrt{2 C_p T_{max} + U_\infty^2} \tag{9}$$

Using this relation in Eq. (4) and again assuming the engine geometry is fixed for cruise at 100,000 ft with dynamic pressures of 50, 100, and 200 lb/ft^2, lines of constant thrust can be plotted in the velocity-altitude plane for a supersonic combustion process. These results are shown in Fig. 5. This plot shows that the thrust available is a strong function of altitude but only a weak function of velocity. Comparing the loci of constant drag lines (thrust required)(Fig. 3) with the loci of constant thrust available lines (Fig. 5), reveals that the critical engine design point is the highest altitude cruise condition desired.

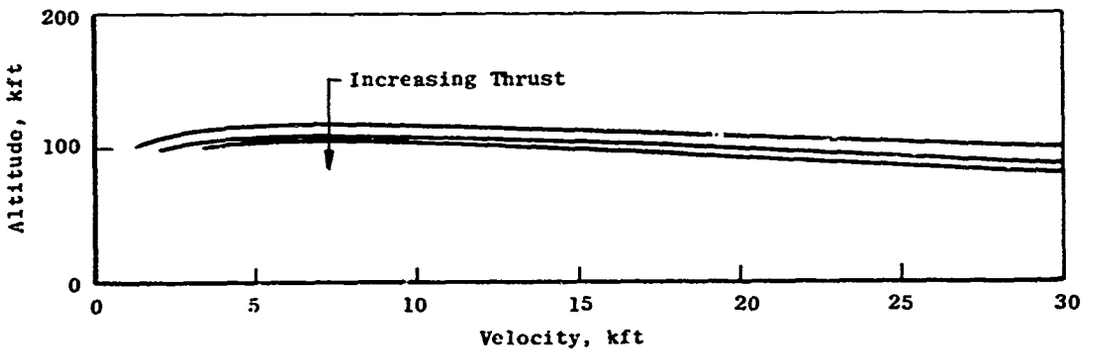

Fig. 5 Representative Altitude-Velocity Relationship for Constant Thrust Available from a Particular Engine—Supersonic Combustion (Eqs. (4) and (9))

2.2 SOME AERODYNAMIC FACTORS IN HYPERSONIC FLIGHT

2.2.1 Aerodynamics of Lift and Drag

In this section, a simple theoretical analysis and typical experimental data are used to emphasize some basic aspects of aerodynamics applicable to high-speed lifting vehicles. Representative literature is referenced so that more thorough study may be facilitated although, as usual, no claim is made for completeness of the references. The aerodynamic force coefficients of primary interest in this study are the lift and drag coefficients, C_L and C_D, respectively, and their ratio, L/D. In general, we shall consider slender, delta-winged or lifting-body aerodynamic shapes such as the typical examples shown in Fig. 6.

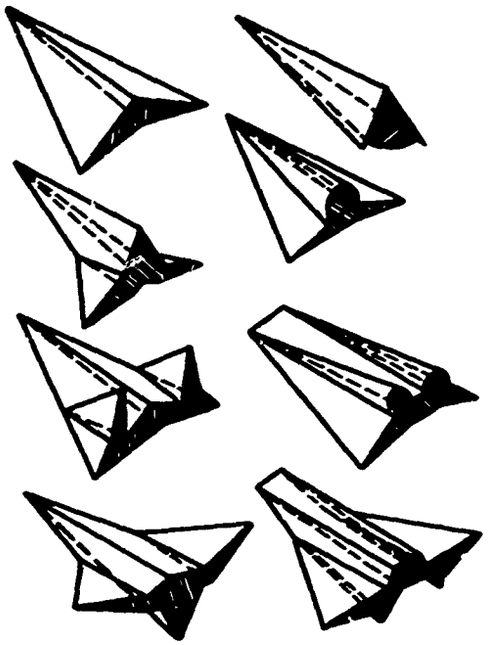

Fig. 6 Examples of Aerodynamic Shapes

It is useful to begin by discussing the lift and drag characteristics pertaining to these shapes. However, it must be remembered that, in addition to physical characteristics and Mach number, the drag coefficient, in particular, becomes dependent upon Reynolds number at the higher flight altitudes. Thus, it is important to withhold judgment of particular configurations until their performance has been evaluated over a broad range of flight conditions. Further, of course, it should be noted that many wind tunnel measurements on these configurations have been made without simulation of operating propulsion systems or considering trim forces, and these can be important factors in the system aerodynamics.

Another form of Reynolds number sensitivity is related to the effect of transition of the boundary layer from laminar to turbulent flow. The location on the body where this occurs is a function of local Reynolds and Mach numbers plus other factors such as surface roughness, pressure gradients (including related crossflow), and wall-to-adiabatic recovery enthalpy ratio, surface mass transfer, vibration, etc. Most of these factors will vary with angle of attack, speed-altitude operation, and configuration. A recent publication on this subject is the symposium proceedings edited by McCauley (Ref. 2, 1971). Under many conditions, boundary-layer separation also will be a factor in determining C_L and C_D. In addition to the pressure gradient forcing separation, most of the same factors that influence transition also must be considered in regard to separation.

Many treatments of the lift and drag of hypersonic bodies have been published. For examples, one may consult Hankey and Elliot (Ref. 3, 1968), Becker (Ref. 4, 1965), and many others. A recent and valuable discussion of the subject has been given by Roe (Ref. 5, 1970), who includes many references with his lecture notes. Numerous NASA reports have given data for a variety of configurations. Among the books containing material on this subject, there is Kuchemann (Ref. 6, 1965). In Fig. 7 an example is presented of theory and measurement relative to a delta wing with blunted leading edges and 75-deg sweep. The experimental data correspond to conditions of high-altitude flight with pronounced low density or viscous effects.

It is interesting to note certain simple relationships which will be outlined here. Consider a flat plate in hypersonic flow at small angle of attack as sketched.

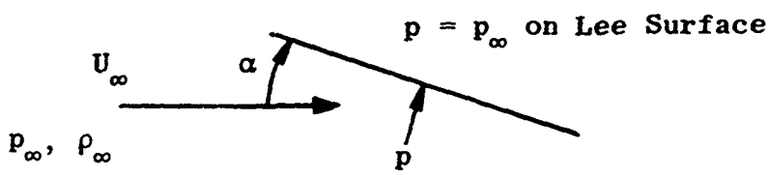

Recalling simple Newtonian theory, the pressure coefficient on a surface impacted by oncoming molecules is

$$C_p = \frac{p - p_\infty}{\rho_\infty U_\infty^2/2} = 2\sin^2\alpha \approx 2\alpha^2 \qquad (10)$$

where α is expressed in radians. Thus, the lift coefficient for small α is

$$C_L = C_p \cos\alpha \approx 2\alpha^2 \qquad (11)$$

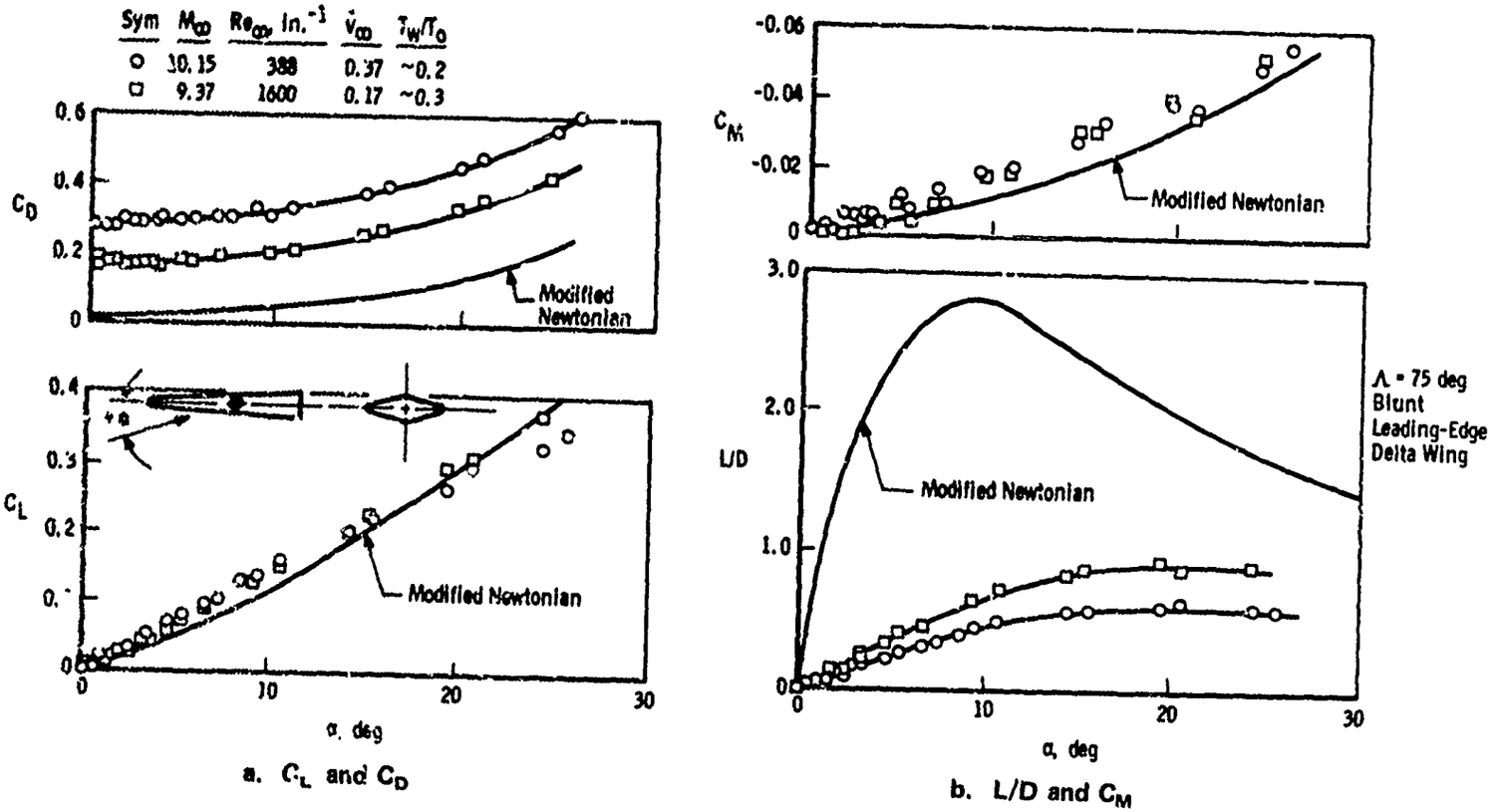

Fig. 7 Delta Wing Aerodynamic Characteristics (Ref. 23)

Similarly, the drag coefficient, assuming inviscid fluid, is

$$C_{D(inv.)} = C_p \sin \alpha \approx 2\alpha^3 \tag{12}$$

Combining Eqs. (11) and (12) gives

$$L/D(inv.) \approx 1/\alpha \tag{13}$$

However, if viscid fluid effects are accounted for, friction drag must be included in the expression for C_D. This may be done by assuming that the boundary layer flow will be laminar at the conditions where friction drag is a dominant factor in determining C_D and L/D and then noting that expressions for the total friction-drag coefficient, C_F, such as might be taken from Luxton and Young (Ref. 7, 1962), suggest the approximation

$$C_F = \frac{0(1)}{(Re_{\delta,\ell})^{1/2}} \tag{14}$$

for hypersonic, laminar small-α conditions. Although $Re_{\delta,\ell}$ denotes local Reynolds number, it is replaced by the free-stream value for simplicity. Then, from Eqs. (12) and (14),

$$C_{D(vis.)} = 2\alpha^3 + 0(1)/\sqrt{Re_{\infty,\ell}} \tag{15}$$

Finally, for a flat plate in hypersonic flow

$$L/D(vis.) \approx \frac{1}{\alpha + \dfrac{1}{2\alpha^2\sqrt{Re_{\infty,\ell}}}} \tag{16}$$

Equation (16) obviously has limited utility, but it is derived here primarily to indicate in a simple way how angle of attack and Reynolds number enter into the determination of L/D at high Mach numbers. In Fig. 8 the L/D from Eq. (16) is plotted for two values of $Re_{\infty,\ell}$. The diminished $(L/D)_{max}$ and the increased angle of attack necessary to attain $(L/D)_{max}$ accompanying decreased Reynolds number are readily apparent.

At high altitudes, where the boundary layer may be considered entirely laminar, the L/D ratio (without assuming $M_\infty \gg 1$) may be correlated with a parameter $\overline{V}_\infty$, where

$$\overline{V}_\infty = M_\infty (C_\infty/Re_{c\infty})^{1/2} \tag{17}$$

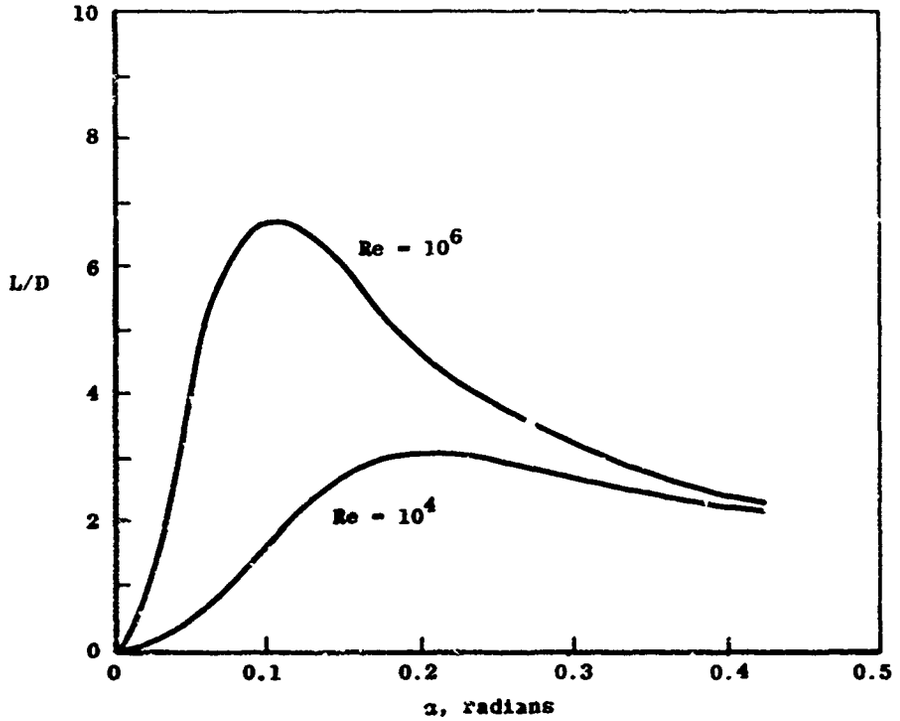

Fig. 8 Lift-to-Drag Ratio of a Flat Plate

An example of this dependence is shown in Fig. 9. For slender vehicles of the type considered here, the L/D dependence illustrated in Fig. 9 is largely caused by a strong dependence of C_D on the parameter $\overline{V}_\infty$. This is also reflected in Fig. 7.

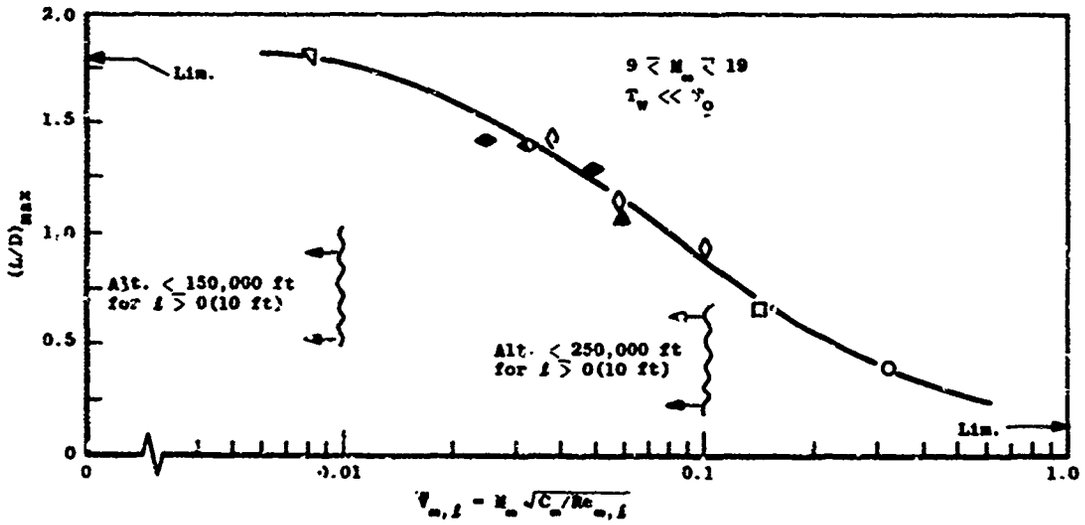

Fig. 9 Lift-to-Drag Ratio of a Slightly Blunted 9-deg Semiangle Cone (Ref. 23)

Another factor to keep in mind in this discussion of the L/D ratio of hypersonic vehicles is the role of form drag or fineness ratio. Another simple two-dimensional theoretical exercise will serve to illustrate this point. In the previous example which was based upon a two-dimensional flat plate, there was no form drag. The flat plate could be described as a body of infinite fineness ratio. Therefore, a body of finite thickness must be considered if the influence of fineness ratio is to be brought out. A wedge-shaped airfoil would serve the purpose, although a biconvex, double-wedge or other shapes could as easily be assumed. With reference to the following sketch which shows a slender wedge-shaped airfoil at small angle of attack, the

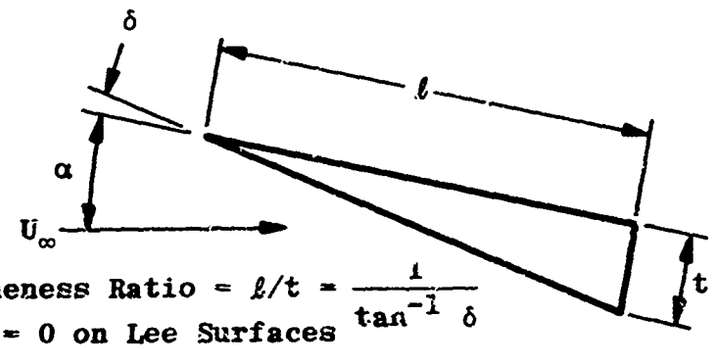

Fineness Ratio = $\ell/t = \dfrac{1}{\tan^{-1}\delta}$

$C_p = 0$ on Lee Surfaces and Base

application of Newtonian aerodynamic theory leads to the expression for pressure coefficient, cf., Eq. (10),

$$C_{p(\text{bottom})} = 2(\alpha + \delta)^2 \tag{18}$$

Then

$$C_L = 2(\alpha + \delta)^2 \tag{19a}$$

$$C_D = 2(\alpha + \delta)^3 \tag{19b}$$

From Eq. (19), for the L/D in inviscid hypersonic flow,

$$L/D = 1/(\alpha + \delta) \tag{20}$$

But

$$\delta = t/\ell = \text{inverse of the fineness ratio}$$

so fineness ratio is a factor in determining the L/D. Equation (20) suggests that L/D should increase with ℓ/t, and this is supported by the experimental data presented in Fig. 10. When load-carrying capacity or internal volume is taken into account, it may develop that shapes of high fineness ratio also have high surface area, with consequent penalty in friction drag. Then, the shape with large $(L/D)_{max}$ at low altitudes may suffer the greater percentage loss in $(L/D)_{max}$ as altitude increases.

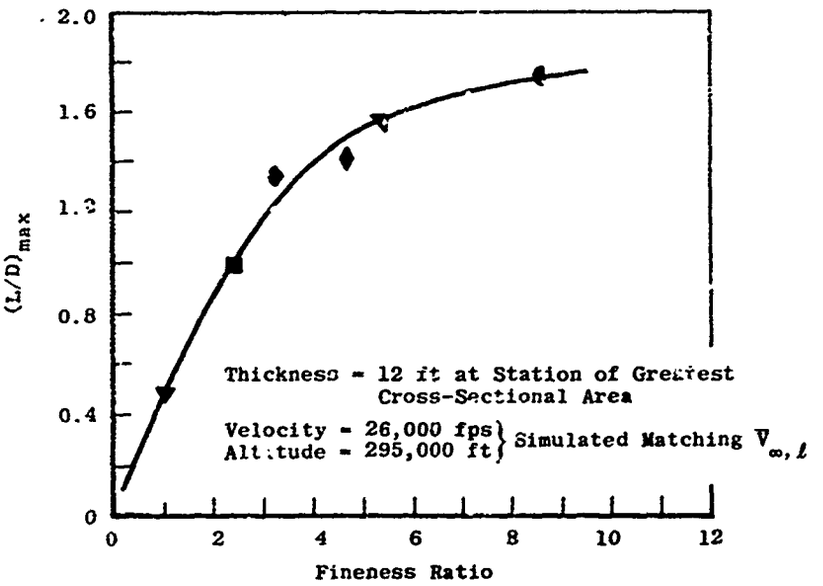

Fig. 10 Qualitative Influence of Fineness Ratio on Lift-to-Drag Ratio at High Altitude (Ref. 23)

2.2.2 Real-Gas Considerations

The previous discussion has ignored the possible effects of real-gas phenomena in the flow around a hypersonic vehicle. Examples of this are presented here with the purpose of allowing some general conclusions or assumptions regarding impact on the rocket plane problem. Although earlier attention was given only to C_L and C_D, the scope of discussion is broadened to include other aerothermodynamic matters in this section. In that way, some of the introduction relevant to later consideration of heat protection and propulsion is provided. Actually, it is shown that the preceding review of basic aerodynamics is not significantly affected when real-gas effects are included. However, local flow-field conditions may be strongly influenced, with corresponding implications in vehicle design.

It is not necessary for our purposes to try to specify precisely the vehicle operating conditions where thermochemical nonequilibrium flow will be encountered. The assumption is made that a rocket plane will be large, perhaps 25 m (80 ft) or more in length. Therefore, there will be opportunity for both equilibrium and nonequilibrium conditions to exist simultaneously in the flow field. Below approximately 20 km (66,000 ft) altitude, or 3 km/sec (10,000 ft/sec) speed, overall equilibrium is a reasonable assumption. For speeds greater than 3 km/sec, at altitudes above 20 km in the continuous flight corridor, nonequilibrium conditions are likely to be widespread.

Figures 11 and 12 show Whalen's (Ref. 8, 1962) calculations of surface pressure and temperature on a wedge-slab wing. The expansion of the flow field following the rather strong shock at the leading edge allows full play to the nonequilibrium effects, and some impressive differences are seen between perfect-gas, equilibrium, and frozen thermochemical flows under the conditions of this example. The corresponding skin-friction and heat-transfer coefficients are shown in Fig. 13. In these examples equilibrium conditions are assumed in the stagnation region.

On the basis of hypersonic small disturbance flow theory, Inger (Ref. 9, 1963) has discussed similitude laws governing inviscid nonequilibrium flows around blunt or sharp-nosed slender bodies at zero angle of attack. He also discusses the effect of a nonequilibrium dissociated free stream such as may exist in a high enthalpy hypersonic wind tunnel. The question of simulation of nonequilibrium real-gas flows in laboratory facilities will not be discussed. However, it is clear that this is an important problem, and a number of important papers have been written on that subject. One of the most recent, which summarizes and references much earlier work, is that by Wittliff and Sundaram (Ref. 10, 1968).

W. S. Norman and J. C. Adams of ARO, Inc., AEDC/VKF, have calculated a number of simple flows for the purpose of comparing perfect- and real-gas results. Figure 14 presents one of their examples. It shows gas temperatures at the edge of the boundary layer on the windward surface of a blunt flat plate at 20-deg angle of attack at velocities and altitudes corresponding to the trajectory which might be followed during reentry from orbital operations.

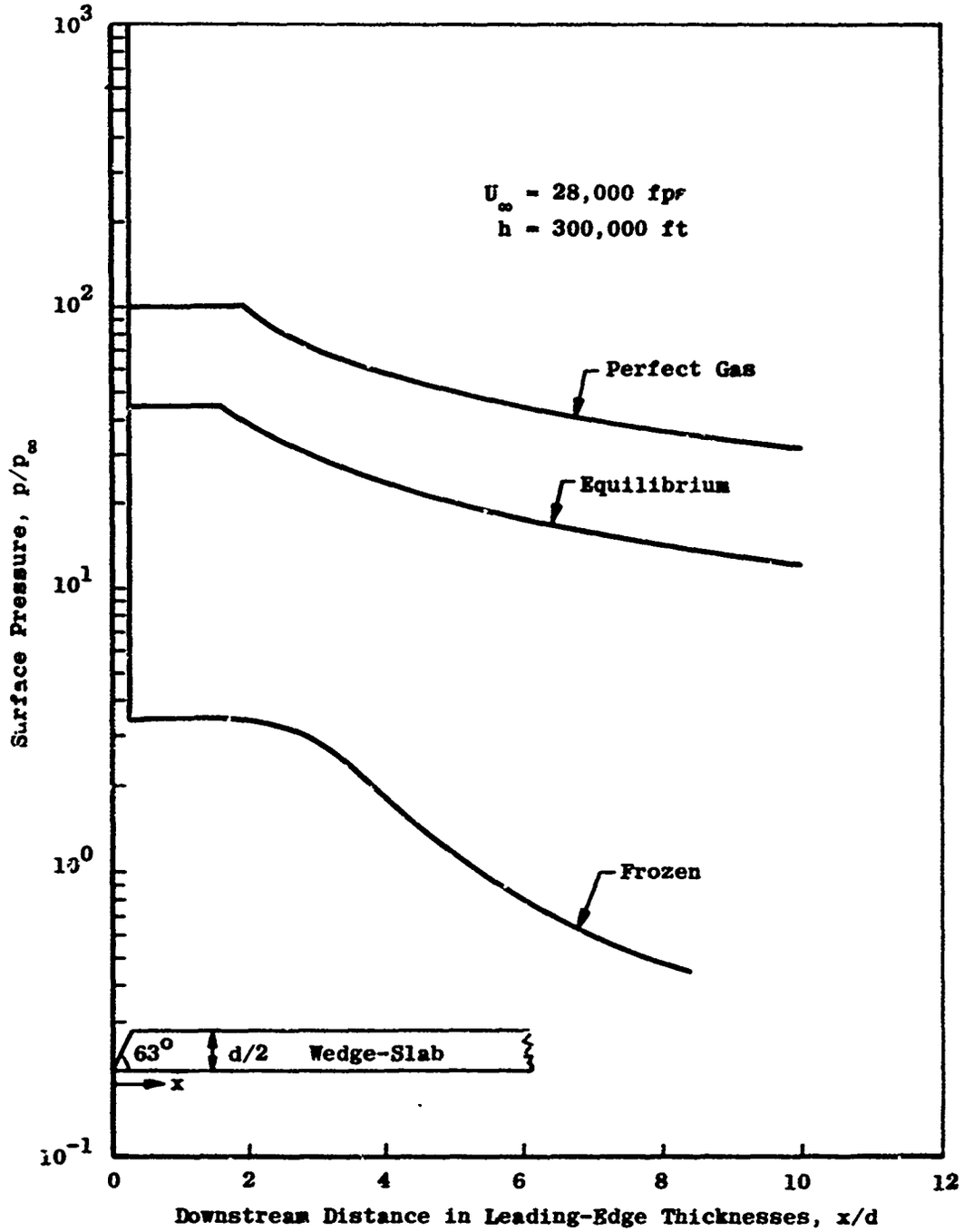

Fig. 11 Example of Influence of Nonequilibrium Conditions on Pressure Distribution

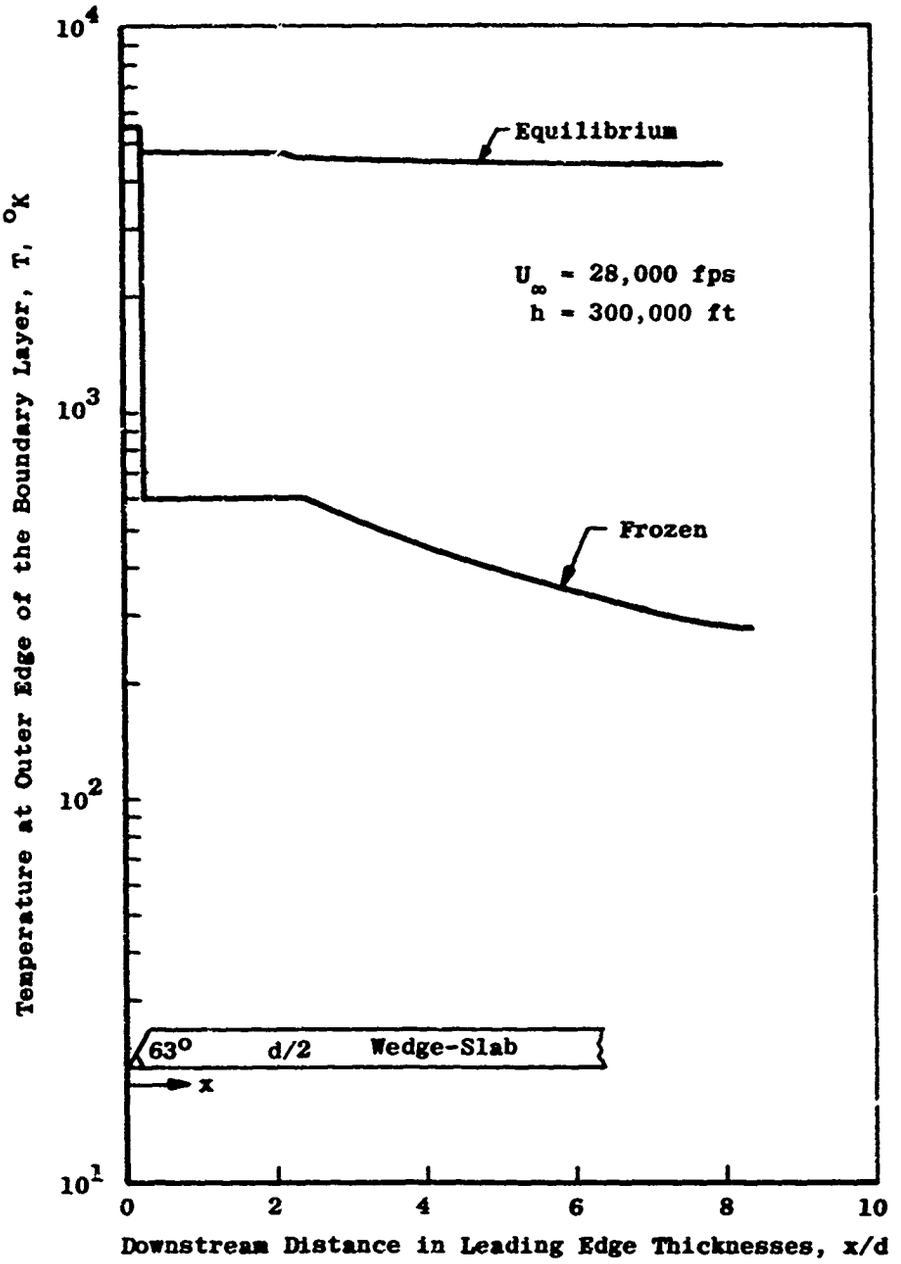

Fig. 12 Example of Influence of Nonequilibrium Conditions on Temperature Distribution

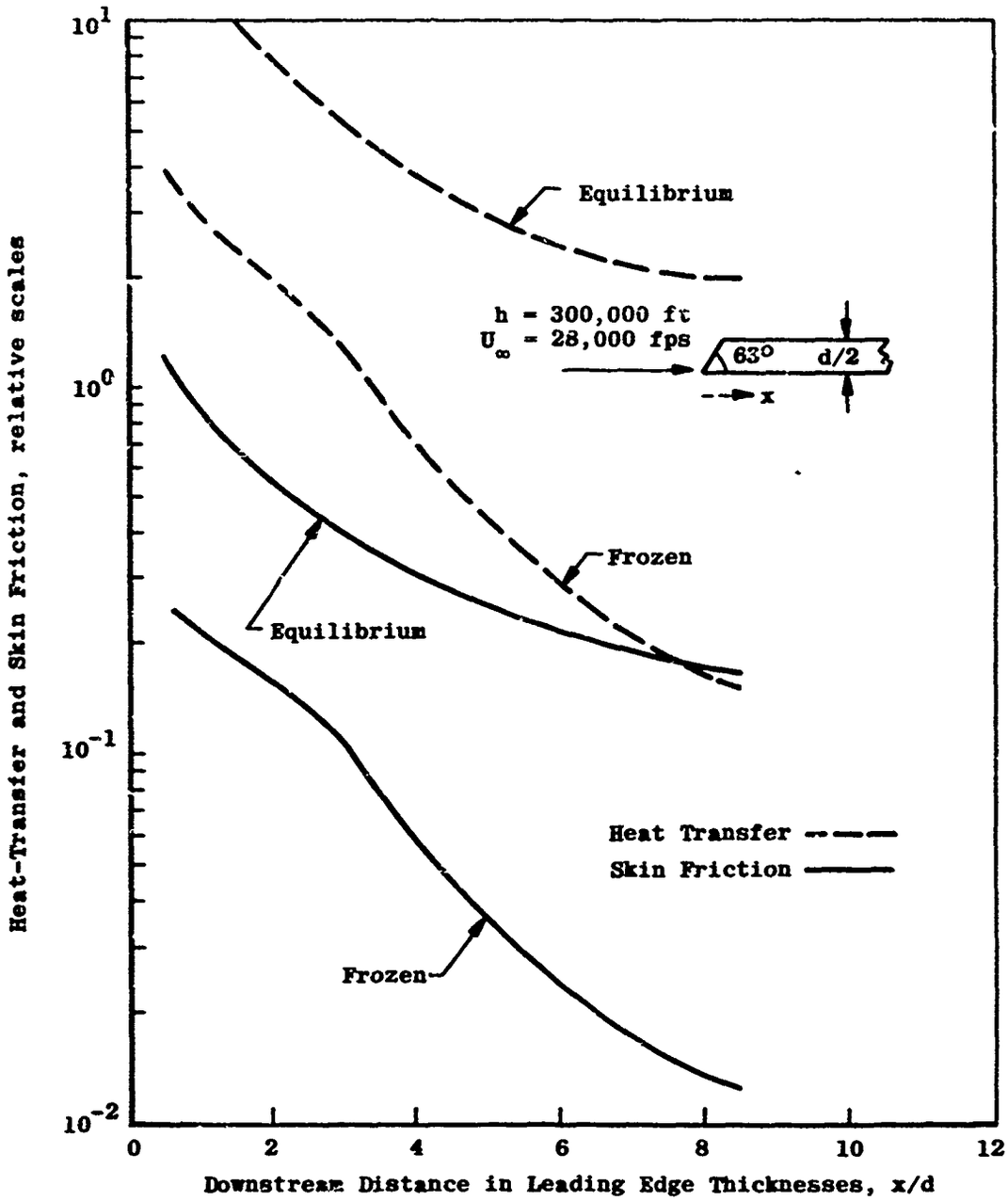

Fig. 13 Example of Relative Effects of Nonequilibrium Conditions on Heat Transfer Skin Friction

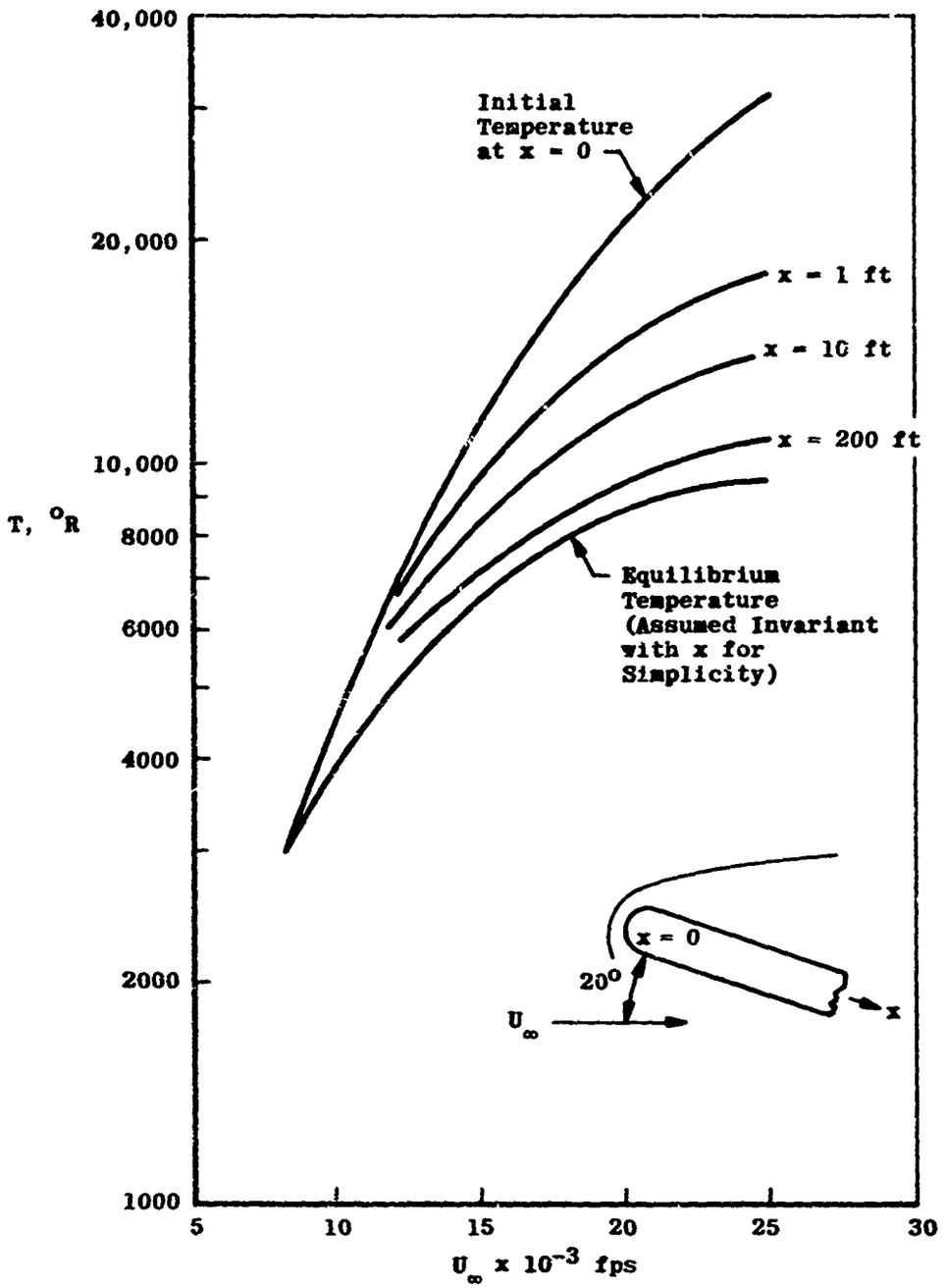

Fig. 14 Example of Approach of Local Static Temperatures Toward Equilibrium Value (from Norman, ARO, Inc.)

The initial shock crossing has been assumed frozen in this problem, and the variation of local temperature with distance downstream along the plate represents the nonequilibrium process which is predicted to exist over a length on the order of 100 ft. This example implies that the length of a large rocket plane may be covered by nonequilibrium flow, with equilibrium being attained near the base. If a sharp flat plate were assumed for this example, the levels of temperature would be reduced, but the length to the attainment of equilibrium would be at least as great, according to these calculations.

In another example calculated by Norman and Adams and shown in Fig. 15, the local heat-transfer rate on a flapped wedge is estimated on the basis of either laminar or turbulent boundary-layer flow and either perfect or equilibrium real-gas behavior. Both real-gas effects and the effect of boundary-layer transition are pronounced in this case.

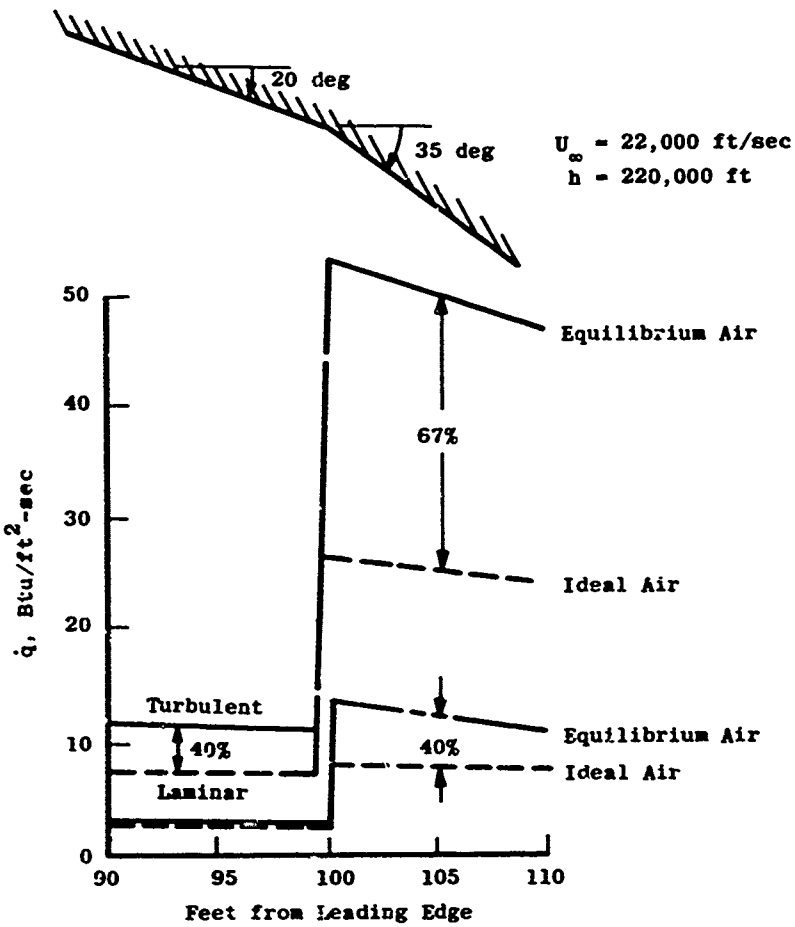

Fig. 15 Heat-Transfer Rate to a Sharp Wedge with a Flap

Remembering that the vehicle under discussion is likely to have a large blunt base, it is interesting to examine real-gas effects on base pressure or base drag. This has already been done by W. S. Norman (Ref. 11, 1969). On the basis of turbulent boundary-layer flow ahead of the base, equilibrium real-gas and perfect-gas base pressure ratios were computed for blunt axisymmetric bodies at zero angle of attack. A result is shown in Fig. 16 where "flight" refers to the real-gas situation and "tunnel," the perfect-gas counterpart. It is seen that at the higher Mach numbers a factor of two or more between base pressures on identical bodies at equal Mach and Reynolds numbers is predicted.

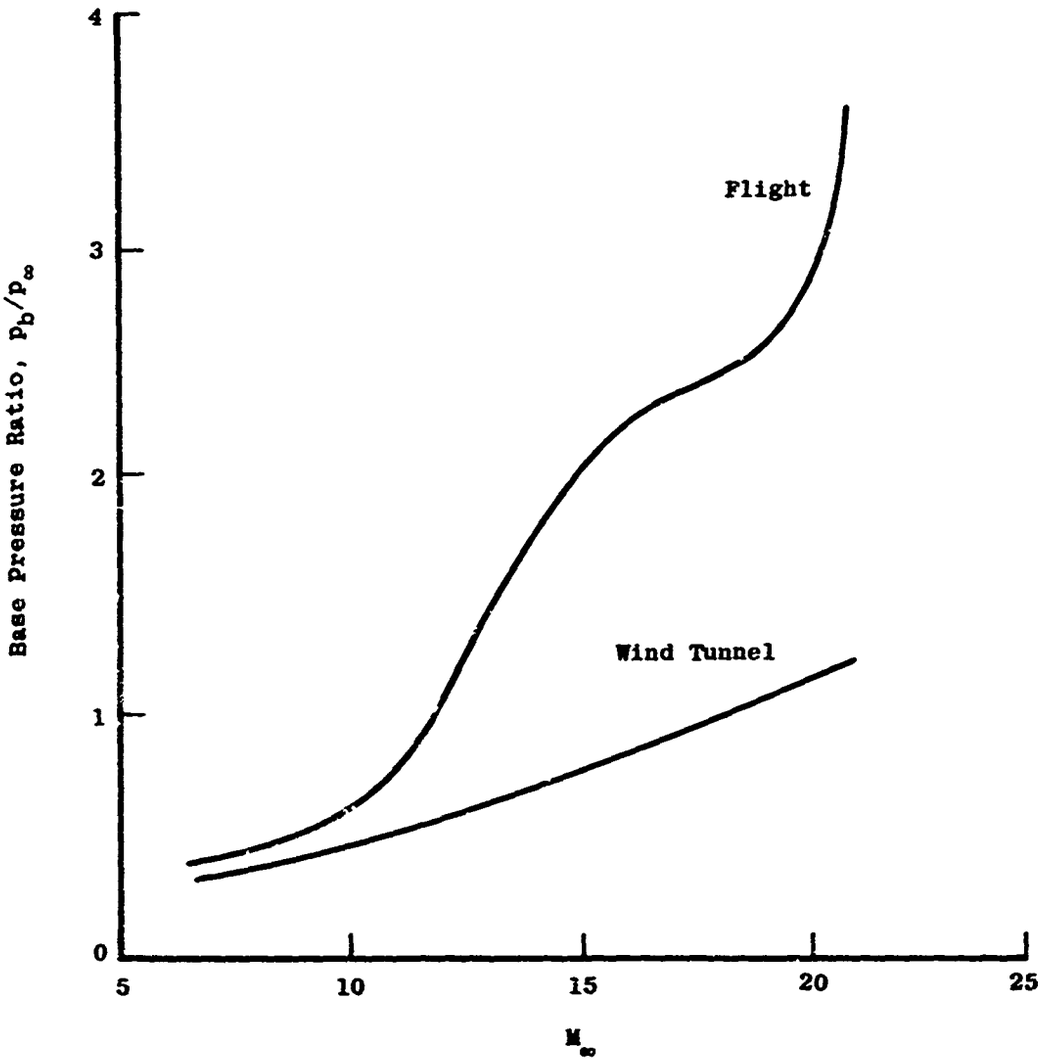

Fig. 16 Example of Real-Gas Influence on Base Pressure Ratio (from Norman, Ref. 11).

Edney (Ref. 12, 1968) has presented experimental data on the effects of shock impingement on heat transfer to blunt bodies. The connection can be seen between this type of investigation and shock impingement phenomena that may be expected in the flow fields of complicated vehicle shapes being discussed. Some quite severe local heat-transfer rates and pressures may be caused by shock impingement. Our purpose in introducing this topic is to mention that real-gas effects also enter into the determination of shock angles, thereby possibly affecting the location of the shock impingement as well as conditions downstream of shock waves. An illustration of the difference between shock angles in real and perfect gases is shown in Fig. 17 which is taken from Bird (Ref. 13, 1958). In this figure note that, first of all, the shock wave angle is less in a real gas. At the greater Mach numbers, the difference between the angles for real and perfect gases varies from the order of 1 deg for a deflection angle of 10 deg to about 7 deg at a deflection angle of 40 deg.

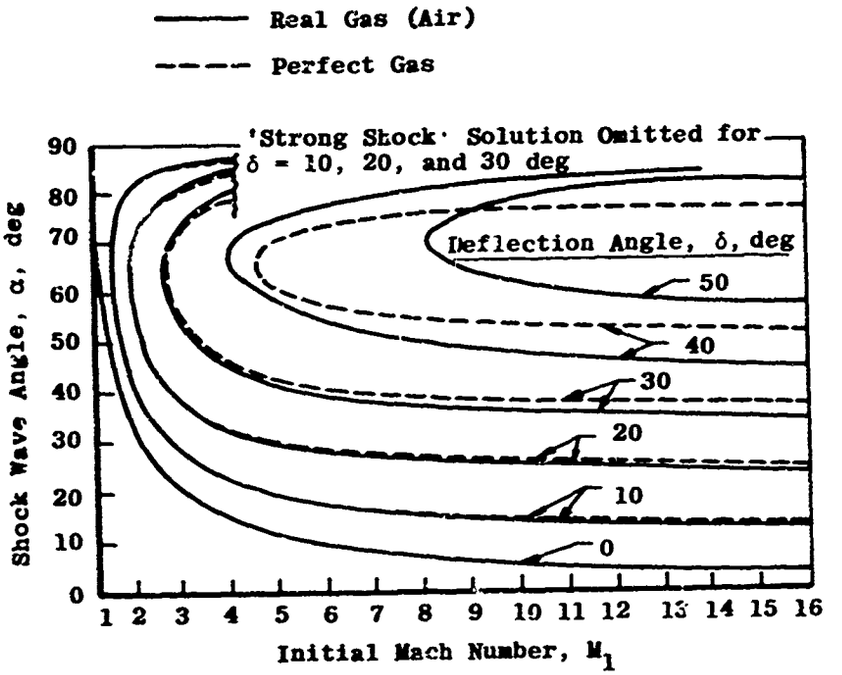

Fig. 17 Oblique Shock Wave Angles

Also of interest are Figs. 18 and 19 which come from Ref. 13. Figure 18 shows that real-gas effects decrease the pressure ratio across an oblique shock wave, in this case calculated for a free-stream temperature of 300°K and a free-stream pressure of 0.01 atm. Figure 19 shows the calculation of the lift of a two-dimensional sharp flat plate for the same free-stream conditions, and it may be seen that the lift coefficient is decreased in real-gas flow. However, it should not be assumed

that real-gas effects always reduce the force coefficients on aerodynamic bodies. For example, when the shock angle is fixed, such as for a normal shock, then the pressure ratio across the shock is greater for a real gas.

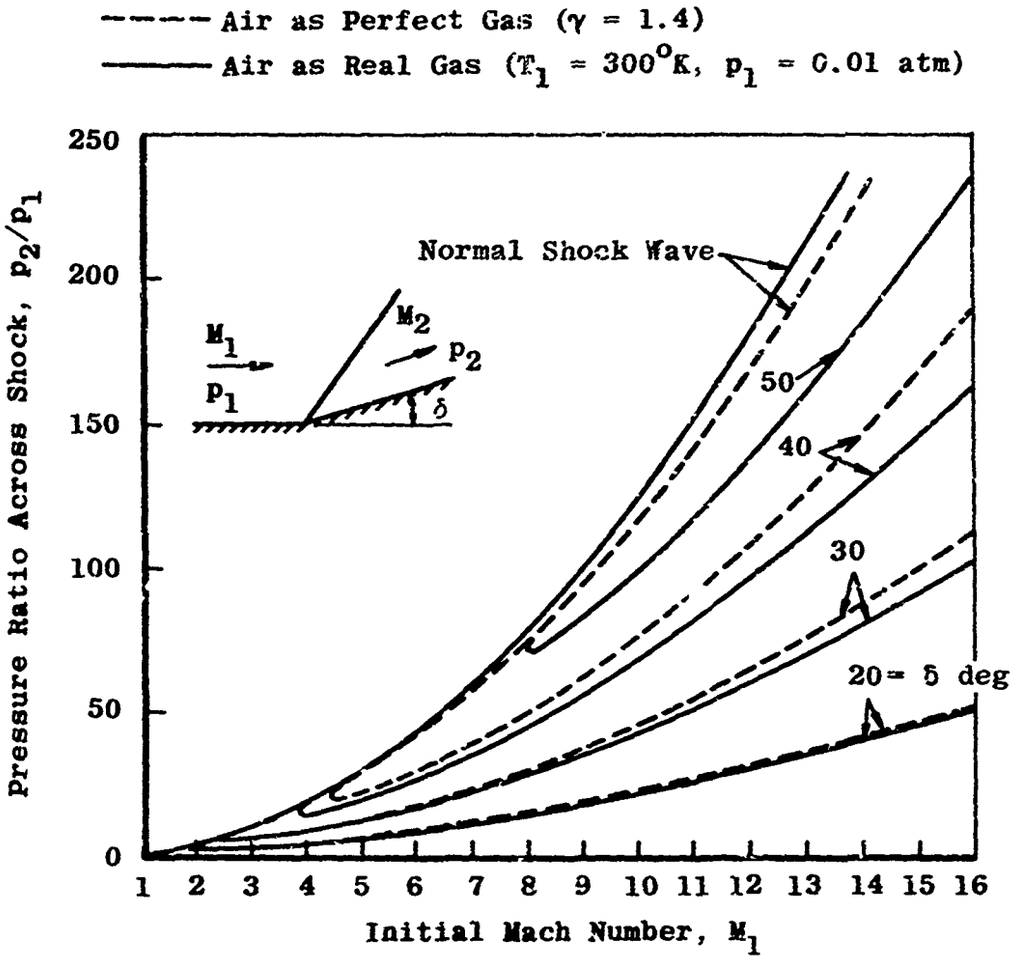

Fig. 18 Pressure Ratio across Oblique Shocks

Another factor to consider is the real-gas influence on local Mach and Reynolds numbers. That subject will not be dealt with, but it is worthwhile to remember that boundary-layer separation and transition may be affected by changes in local Mach and Reynolds numbers occasioned by real-gas behavior.

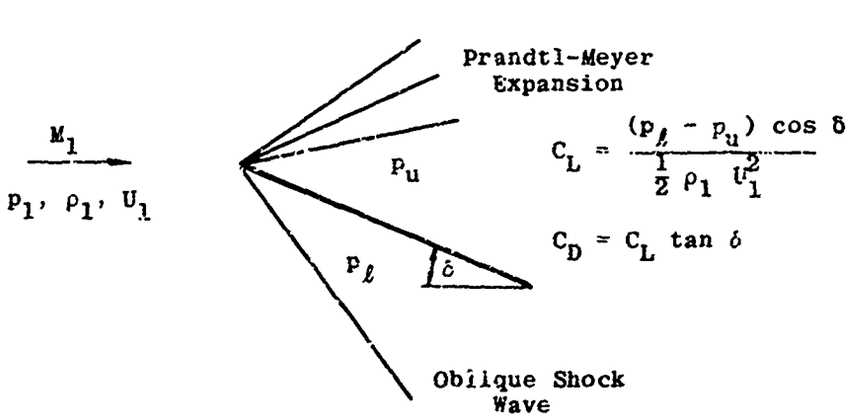

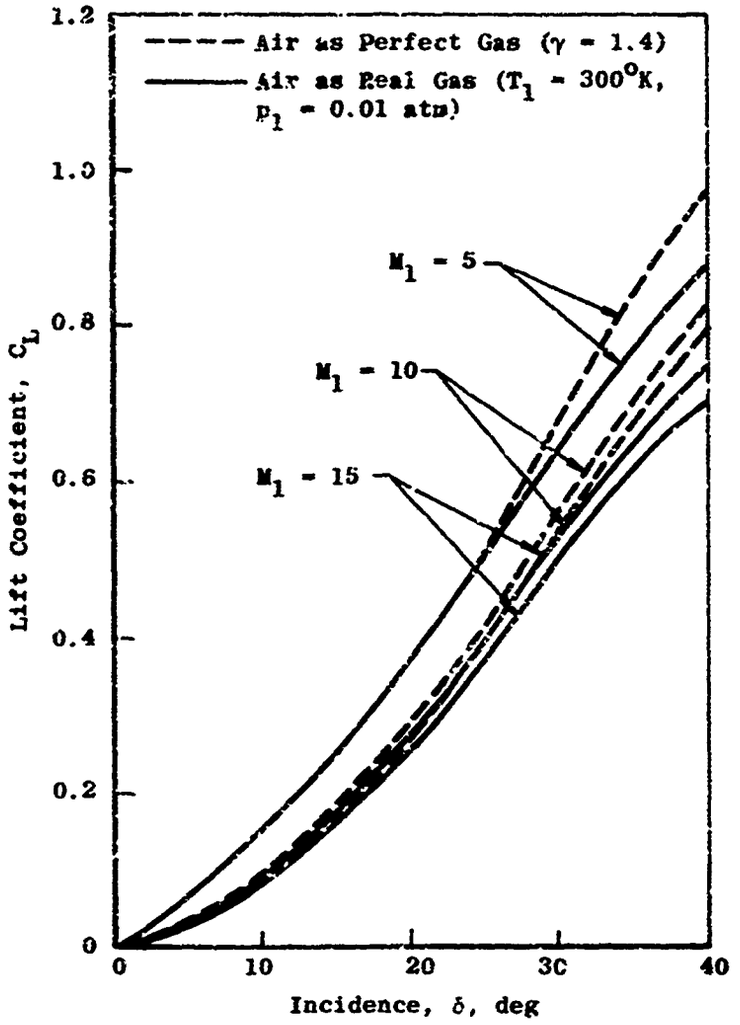

Fig. 19 Lift of Flat Plate

Zienkiewicz (Ref. 14, 1957), Feldman (Ref. 15, 1957), and Romig (Ref. 16, 1959) have dealt with the real-air flow over sharp cones at zero angle of attack. Pressure increases across normal shocks are greater in real air than in a perfect gas with $\gamma = 1.4$. However, sharp-cone surface pressure coefficients and shock angles are less in real air. Recall that the density ratio, ρ_s/ρ_∞, is limited to a maximum value of 6.0 when $\gamma = 1.4$ and note in Fig. 20 that shock angles continue to decrease as real air density ratios exceed 6.0. For cone semi-vertex angles less than 20 deg, there is only a small influence on surface pressure. However, even for the smaller cone apex angles there is a significant effect on surface temperature and density at high speeds. It follows that the inviscid drag coefficient of sharp, slender cones is only slightly affected by real-air behavior, even at hypersonic Mach numbers. Romig shows that, in air

$$C_p/\sin^2\delta \approx 2.07 \tag{21}$$

for a broad range of the parameter $M_\infty \sin\delta$ when the calculation is based on a free-stream pressure of 0.01 atm and free-stream temperatures of 220 to 280°K. Very little effect would be expected from changed free-stream conditions corresponding to different altitudes in the earth's atmosphere. It is seen that this result is very close to the Newtonian flow theory. Bird's result for wedges (Fig. 18) is approximately

$$C_p/\sin^2\delta \approx 2.3 \tag{22}$$

when calculated for real-air free-stream conditions of 0.01 atm and 300°K. Although the effect has not been evaluated, it is important to note that the calculations of Romig and Bird were based on different real-air gas properties. A part of the difference in the coefficients presented here may arise from this use of different air properties.

2.2.3 Aerodynamic Configurations

It may be expected that the aerodynamic vehicle under discussion would generally resemble the delta-winged space shuttle designs much in evidence in the literature at present or the similar hypersonic cruise vehicles described in recent papers. However, attention should also be directed to the Nonweiler wing which has attracted scant interest in the U. S. Nonweiler (Ref. 17, 1963) suggested that easily calculated two-dimensional flow fields may be used to develop families of three-dimensional lifting bodies supporting plane shock waves. These are often referred to as waveriders, and one class of these bodies has been called caret wings. The concept of the Nonweiler wing may be illustrated

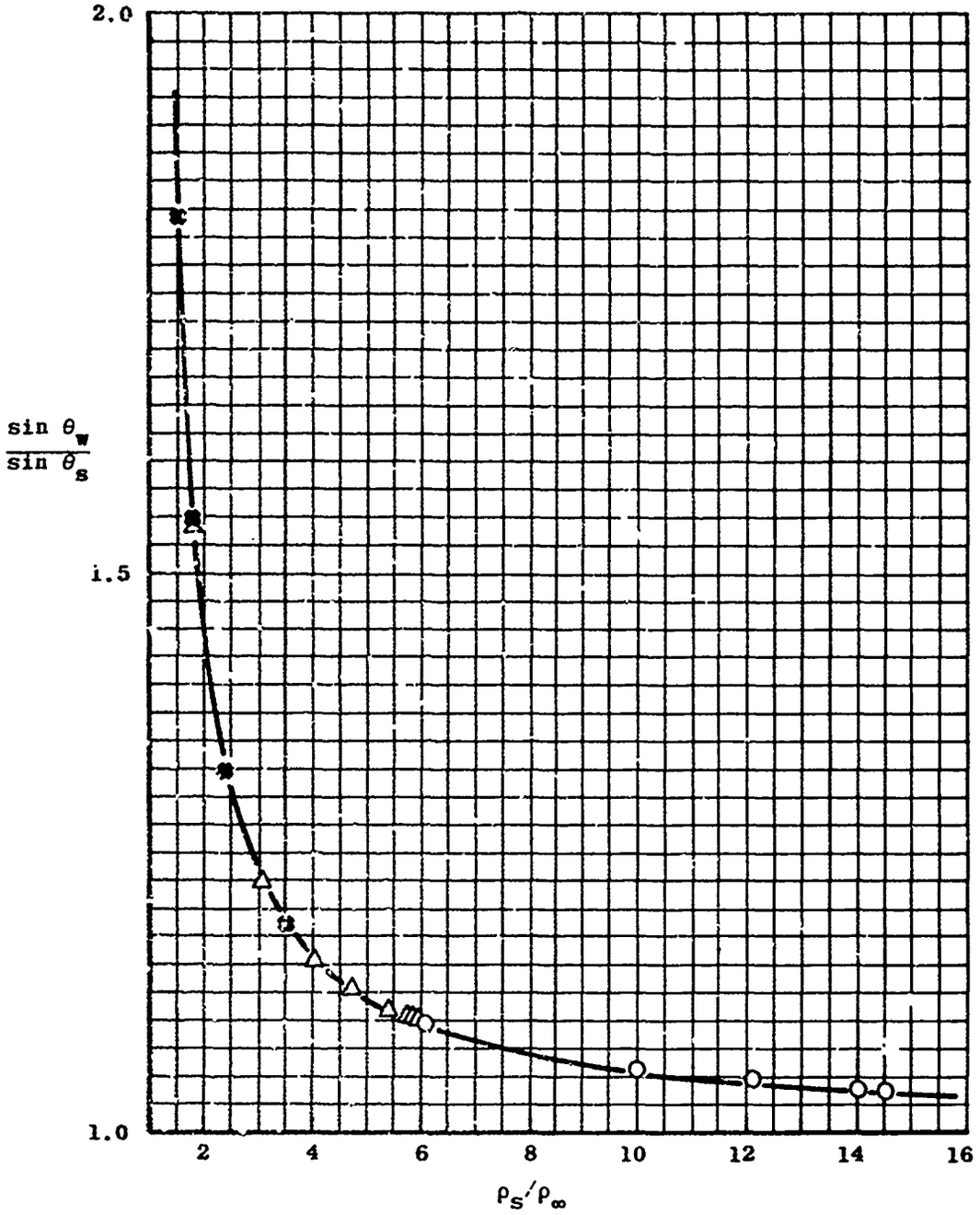

Fig. 20 Correlation of Shock Angles and Density Ratio for Cones in Real Air

by considering the flow past a two-dimensional wedge, the top of which is aligned with the free stream. Mach number is such that the shock wave is attached to the leading edge, as shown in Fig. 21. The flow will not be disturbed if the two-dimensional wedge is converted to a three-dimensional body by forming a solid surface from some of the parallel stream lines in the two-dimensional wedge flow field, as illustrated in Fig. 21. This method can be extended to more complicated bodies, some of which are referred to as W-wings. (See Pike, Ref. 18, 1970), Roe (Ref. 5, 1970), and Roe, et al. (Ref. 19, 1971), for discussion of such shapes.

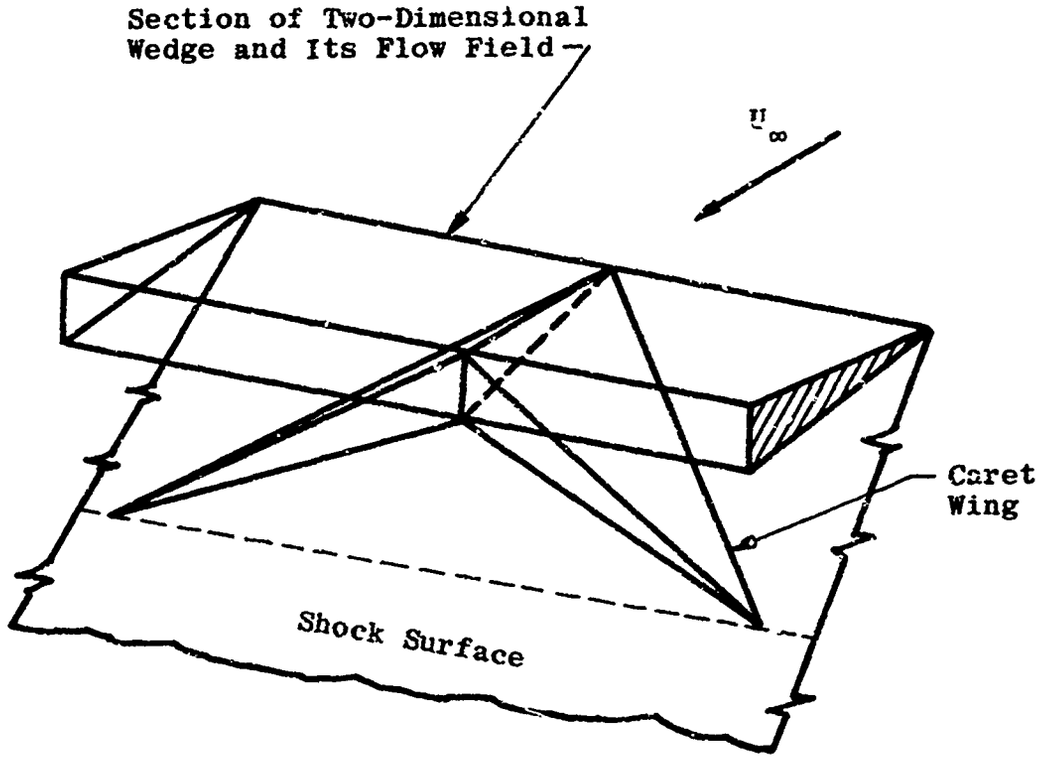

Fig. 21 Caret Waverider Concept

It can be seen that the ability of the Nonweiler wing to contain the windward-side flow without spillage ahead of the trailing edge implies a higher lift coefficient for equal incidence (Ref. 20, 1970). Figure 22 presents the windward-side pressure coefficient for two-dimensional wedge flows containing plane shock waves. High Mach number and constant specific heat ratio of 1.4 are assumed. The upper curve in Fig. 22 represents the theoretical performance of caret wings in inviscid flow. Also shown in Fig. 22 is the pressure coefficient that would be calculated by Newtonian theory for the same case. The Newtonian pressure coefficient should be a good approximation for the

centerline of a conventional delta wing at incidence, although some loss in pressure coefficient would be expected off of the centerline. Maikapar (Ref. 21, 1967), using Newtonian theory, has treated optimum wing shape selection as an extremum problem and obtained maximum L/D ratios very near to those computed for Nonweiler wings. Townend (Ref. 22, 1970) presents data showing that such aerodynamic advantages are realized in practice. He concludes that the Nonweiler wing may provide lift coefficients greater than those of the convex or flat-bottomed delta shapes which have received most of the attention in the U. S. Roe (Ref. 5, 1970) has reviewed a number of aerodynamic design techniques applicable to optimum shapes in hypersonic flows.

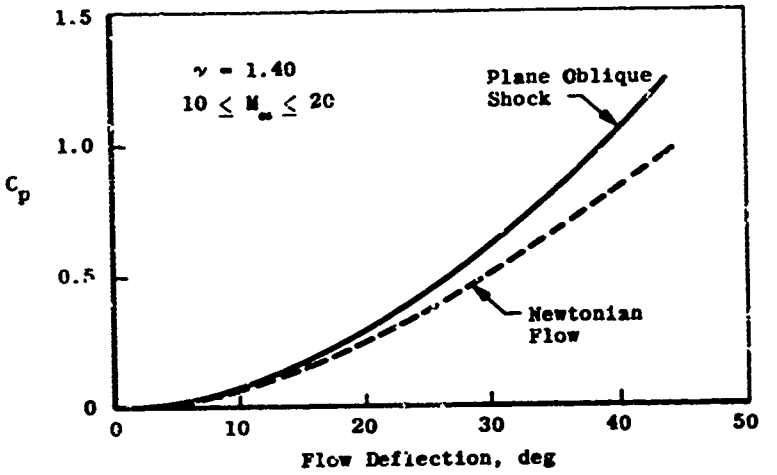

Fig. 22 Plane Oblique Shock and Newtonian Flow Pressures on Windward Surface of Wedges

Other discussion of aerodynamic configurations for hypersonic flight is to be found in the article by Kuchemann (Ref. 6, 1965). From Ref. 6, the uniform pressure coefficient over the lower surface of a simple Nonweiler caret wing is

$$C_p = (4/\gamma + 1)(\sin^2 \sigma - 1/M_\infty{}^2) \tag{23}$$

where σ is the shock deflection angle shown in Fig. 23. The angle of incidence, θ, which may also be interpreted as the effective wedge angle, δ, of the windward surface, is related to σ as follows for an ideal gas:

$$\theta = \sigma - \tan^{-1} \frac{2 + (\gamma - 1)M_\infty{}^2 \sin^2 \sigma}{(\gamma + 1)M_\infty{}^2 \sin \sigma \cos \sigma} \tag{24}$$

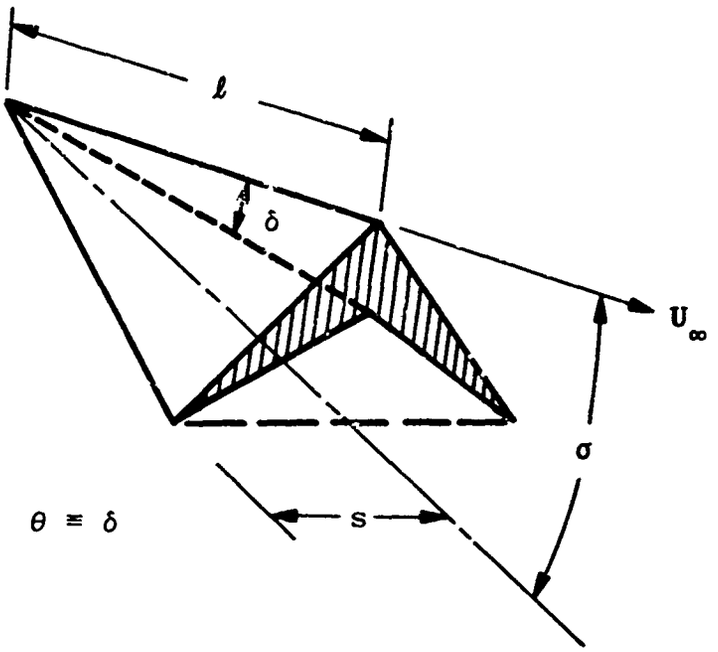

Fig. 23 Nomenclature for Caret Wing

It may be noted that a simpler expression for C_p on a wedge is available from hypersonic small-disturbance theory, viz.,

$$C_p = \theta^2 \left[1.2 + (1.44 + 4/M_\infty{}^2\theta^2)^{1/2}\right] \tag{25}$$

To describe a simple caret wing, it is only necessary to define

s/ℓ = semispan-to-length ratio

r = volume/$S^{3/2}$

S = projected planform area

= $s\ell$

δ = wedge angle

Thus, the lift coefficient of a caret wing is

$$C_L = C_p \cos\theta = \frac{C_p}{(1 + 9r^2\, s/\ell)^{1/2}} \tag{26}$$

and the wave-drag coefficient, including effects of both volume and lift, is

$$C_{D_w} = C_p \sin\theta = \frac{3\,C_p\,\tau\,(s/\ell)^{1/2}}{(1 + 9\tau^2\,s/\ell)^{1/2}} \tag{27}$$

Together they yield an L/D ratio in inviscid flow,

$$L/D = \cot\theta = \frac{1}{3\tau(s/\ell)^{1/2}} \tag{28}$$

Finally, the L/D ratio with skin-friction drag included is

$$L/D = \frac{1}{3\tau(s/\ell)^{1/2}\left[1 + C_F(S_w/S)\dfrac{(1 + 9\tau^2\,s/\ell)^{1/2}}{3\,C_p\,\tau\,(s/\ell)^{1/2}}\right]} \tag{29}$$

where S_w = wetted area. Note that $C_p = 0$ is assumed for lee surfaces. From Eq. (14), for a nominal local Reynolds number $Re_1 = 0\,(10^6)$, $C_F = 0\,(0.001)$ would be a reasonable choice.

The penalties of viscous interaction in regard to hypersonic L/D ratios of a delta wing already have been illustrated, using data from Boylan and Potter (Ref. 23, 1967). A recent comprehensive review of viscous interactions has been given by Korkegi (Ref. 24, 1971). The effects of the decreased high-altitude aerodynamic performance have been analyzed by Hidalgo and Vaglio-Laurin (Ref. 25, 1967). Unfortunately, it is to be expected that the greater wetted area and the viscous corner flows typical of caret and W-wings will suffer higher viscous drag, and therefore their attractive inviscid L/D ratios will decrease rapidly under lower Reynolds number or higher altitude conditions. In this context, the theoretical inviscid flow advantages of W-wings over caret wings and of both over flat-bottomed delta wings may disappear at high Mach numbers and high altitudes, as pointed out by Pike (Ref. 18, 1970) and others. Experimental illustration of this has been furnished by Koppenwallner (Ref. 26, 1971). Figure 24 is taken directly from his paper. The deleterious effects of high Mach number, low Reynolds number conditions on the aerodynamic performance of the more sophisticated bodies, coupled with considerations of aerodynamic heating and structural design, point to the need for including experiments for the entire range of Mach and Reynolds numbers in a thorough evaluation of candidate configurations for an upper stage rocket plane. Configurations which appear best at lower Mach numbers may be much less attractive under conditions of hypersonic high-altitude flight. The more slender or complex shapes also are likely to have less favorable payload volumes.

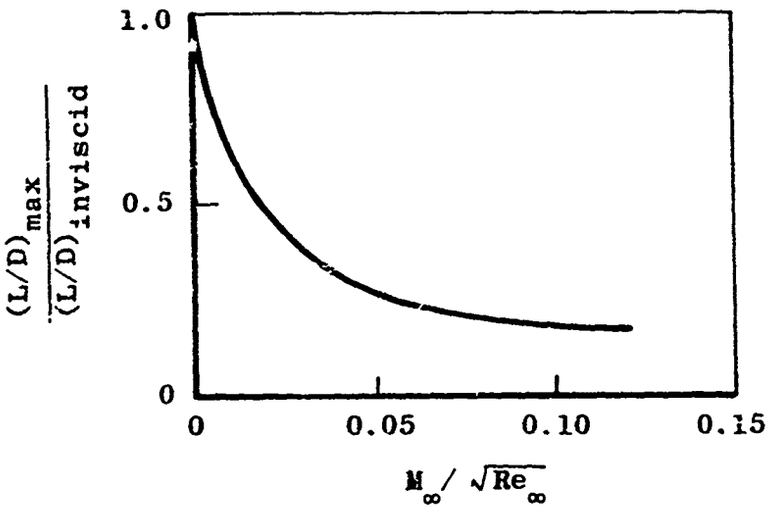

Fig. 24 Koppenwallner's (Ref. 26) Example of Viscous-Flow Effect on a Caret Wing

Analyses of waveriders formed with the use of circular cones and conical shocks have appeared in the English and Russian literature, cf. Jones (Ref. 27, 1963), Pike (Ref. 28, 1970), and Keldysh (Ref. 29, 1968). They have considered the body formed when a circular cone at zero angle of attack is segmented and equipped with triangular wings with their leading edges lying along the conical shock formed by the basic body, as illustrated in Fig. 25. At high Mach numbers, the variation of pressure between the conical shock and the cone surface may be neglected for approximate analysis. Then if the pressure coefficient on the bottom of the wing is assumed to be the same as on the conical sector, the analysis is particularly simple. An estimate of the error in this assumption may be made by alternately considering the pressure everywhere on the bottom of the wing equal to the pressure immediately behind the conical shock. The maximum L/D ratio of a conical sector with a wing is reached when the sector half-angle $\phi < \pi/2$.

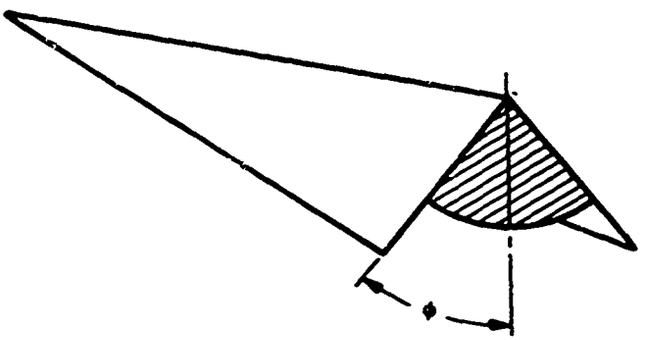

Fig. 25 Proposed Body Shape

Maikapar (Ref. 30, 1966), has discussed bodies formed with the use of intersecting plane and conical shock waves. Keldysh and Maikapar (Ref. 31, 1969) have presented a broad discussion of aerodynamic shapes derived from the combination of plane and conical flow elements. They compare the aerodynamics of different configurations with given volume and planform area at a given Mach number and altitude ($M_\infty = 10$). Bodies of star-shaped cross section are formed of plane shock flow fields separated with longitudinal ribs. Gonor in a series of papers (Refs. 32 through 37, 1963–1968) has developed the subject of star-shaped bodies. Gonor et al. (Ref. 37) have confirmed the theoretical advantages of the star-shaped body in experiments at Mach numbers of 6 and 8 in a wind tunnel. Gonor (Ref. 35) described a hypersonic delta biplane for which he calculated L/D of 3.18 at infinite Mach number. This substantially exceeds the maximum L/D of an elliptic cone of equivalent volume and span.

Up to this point, the discussion of configurations has included only bodies with a swept-back planform such as the delta wing or arrow wing. Actually, unswept leading edges have been considered, for example, by Keldysh and Maikapar (Ref. 31, 1969) and Hankey (Ref. 38, 1970). Hankey develops two optimized wings with approximately equal L/D ratios. One is a wedge with nearly rectangular planform, and the other is a very slender segmented cone with a triangular planform. The reliability of his calculations is supported by experimental data shown to be in close agreement with his theoretical predictions for one case of an optimized lifting body having an unswept leading edge and a low-aspect-ratio planform. The maximum L/D predicted and measured at $M_\infty \approx 14$ and $Re_\infty \approx 10^6$ was approximately 3 at an angle of attack of 2 deg. Considering that a body of the size of 0 (100 ft) in length would have $Re_\infty = 0(10^6)$ at roughly 220,000-ft altitude, this L/D ratio is impressive.

Several other considerations in the selection of an aerodynamic configuration are brought out when problems associated with aerodynamic controls, payload, heat protection, integration with propulsion systems, and low-speed handling are considered. These questions will not be discussed here, although it is very important to remember that any operational craft must be compromised by practical requirements. Some of the numerous recent references that may be consulted in this regard are Keldysh and Maikapar (Ref. 39, 1970); Maikapar (Ref. 40, 1968), Eggers et al. (Ref. 41, 1970), Henry and McLellan (Ref. 42, 1971), Townend (Ref. 43, 1966), Small et al. (Ref. 44, 1970), Neumann (Ref. 45, 1970), and Ceresuela (Ref. 46, 1970). A large section of the AIAA publication Astronautics and Aeronautics (Vol. 9, No. 2, Feb. 1971) is devoted to a series of papers on space shuttle technology, and the August 1971 issue of this same journal has several papers on hypersonic aircraft.

2.2.4 Flow Separation

The subject of flow separation and development of vortices on the leeward side of delta wings has been covered in a number of recent papers. The proceedings of the AGARD conference on Hypersonic Boundary Layers and Flow Fields (AGARD CP No. 30) almost serves as an appendix for the present paper. Of the other most recent publications, there are Whitehead (Ref. 47, 1970), Rao (Ref. 48, 1971), and Whitehead and Bertram (Ref. 49, 1971).

In addition to the type of flow separation discussed in those papers, there is the possibility of flow on either leeward or windward surfaces being separated because of interaction with the exhaust plume of the propulsion unit or, e.g., control surfaces. Papers related to this problem have been written, for example, by Cubbage et al. (Ref. 50, 1971), McGhee (Ref. 51, 1970), Fong (Ref. 52, 1971), and Boger et al. (Ref. 53, 1971). The influence of wall blowing or mass transfer has been discussed by Hartunian and Spencer (Ref. 54, 1967), Kubota and Fernandez (Ref. 55, 1968), Pappas and Lee (Ref. 56, 1970), Marvin and Akin (Ref. 57, 1970), and a number of others.

Pappas and Lee show that for a given value of the blowing parameter, $\dot{m}/(\rho_\infty U_\infty)$, the surface pressure downstream of the nose on a blunt cone is increased much more when the injected gas has a low molecular weight. Marvin and Akin show that mass transfer decreases boundary-layer transition Reynolds number according to the empirical correlating expression

$$Re_{\delta,t} = (Re_{\delta,t})_{F=0}\left[1 - 0.25(M_{air}/M_{injectant})^{0.25}F\right]$$

where F is the parameter expressing the ratio of blown mass flux to the free-stream mass flux. Presumably then, injection of gases of lower molecular weight would have a stronger tendency to separate a laminar boundary layer because of the increased pressure rise, but if the boundary layer underwent transition to turbulent flow more readily for the low molecular weight transpired gas, boundary-layer separation might actually be delayed. The role of surface mass transfer in regard to convective heating, boundary-layer transition, boundary-layer separation, and external combustion may be very complicated indeed.

Whitehead and Bertram (Ref. 49, 1971) have shown that the formation of longitudinal vortices on the leeward side of delta wings at angles of attack is inhibited if the wing planform is parabolic or hyperbolic instead of the more common round-nosed triangle. Apparently, the avoidance of discontinuity in planform leading-edge curvature through the use

of the pure analytic shapes accounts for the effect they have found. Rao (Ref. 48, 1971) found a similar inhibition of the formation of vortices when he deflected the tip downward on a conventional triangular delta wing at an angle of attack, i.e., made the lower surface concave.

2.3 PROPULSION SYSTEM

2.3.1 Configuration

For hypersonic vehicles, a dominant design consideration in addition to external aerodynamics discussed in the last section results from the emergence of hydrogen as an attractive fuel above Mach 7 (Hankey, Ref. 38, 1970). Specifically, liquid hydrogen has a low density resulting in a requirement for large storage volume. This translates into the design requirement of minimum surface area per unit internal volume and has resulted in the conception of the all-body vehicle for a single-stage hypersonic transport or for the first stage of a two-stage configuration. An example of such a body shape is a delta planform with elliptical cross sections.

A typical upper stage then may be a propulsive lifting body having an approximately triangular planform with leading edges inclined downward (waverider) or simply a concave lower surface. A potential feature of such an aircraft is the production of thrust by direct heat addition to part of the airstream. This has been discussed by Kuchemann (Ref. 6, 1965), Townend et al. (Ref. 58, 1970), Billig (Ref. 59, 1967), Kallergis (Ref. 60, 1969), Quick (Ref. 61, 1969), and Maurer et al. (Ref. 62, 1970).

In view of current and projected engine technology, it appears that no single type of air-breathing engine can fulfill the requirements of a hypersonic aircraft. Turbine engines are presently limited to about Mach 3.5, whereas a subsonic combustion ramjet may operate in the Mach number range from 1 to 6. Above Mach 6, supersonic combustion ramjets are more efficient and produce more thrust. Furthermore, if orbital capabilities are envisioned, auxiliary rocket engines are required. It must be concluded then that a composite propulsion system will characterize the earlier autonomous aircraft which cruise at hypersonic speeds. Weights may range from 500,000 to 3,000,000 lb at take off for complete systems. Second stages may weigh between 200,000 and 800,000 lb. Payloads may be between 20,000 and 60,000 lb.

The thrust of an air-breathing engine is limited by the amount of heat that can be added to a quantity of air. The low-temperature limit of the cycle is the combustor inlet temperature, whereas the high-temperature limit is the combustion temperature. As flight speeds approach Mach 7 to 8, deceleration of the flow to subsonic values results in temperature rises on the order of 3500°R. At such temperatures, the burning of fuel is accompanied by a high degree of dissociation and consequently results in little contribution to useful work or thrust. However, if inlet diffusion is limited so that the flow is still moving at supersonic speed as fuel is injected, combustion takes place at a lower temperature, and the energy addition produces thrust rather than being dissipated in dissociating molecules. Thus, the supersonic combustion ramjet or external-burning engine is capable of competing in the Mach 7 to 15 regime now occupied exclusively by the rocket.

In a scramjet, combustion can occur in a fixed geometry burner-nozzle combination through a large range of combustor inlet Mach numbers. Because the Mach number entering the burner is permitted to vary with flight Mach number, the inlet and therefore the complete engine does not require variable geometry. Such an engine can operate over a large range of flight Mach numbers, and consequently is very attractive as an accelerating engine. In contrast, the subsonic combustion ramjet requires complex variable inlets and nozzles to operate efficiently over a wide Mach number range, and the structural weight and complexity of such components increase sharply with Mach number. Dual-mode or "convertible" ramjets, which can operate with either subsonic or supersonic burning, hopefully combine the best features of both.

At least six research scramjets have been built and ground tested in the United States. Performance experiments on the complete engine have demonstrated repeatedly stable and controllable combustion mode conversion, efficient operation, successful ignition techniques, and substantiated aerothermodynamic design procedures. The conclusion is that there is no major obstacle to the development of the scramjet propulsion system. There is, however, a complex of problems involved in developing a scramjet that is optimally integrated with the configuration and structure of a hypersonic aircraft.

2.3.2 Fuels

The operating characteristics of all hypersonic aircraft propulsion systems are strongly dependent upon the fuel used. Hydrocarbon fuels such as kerosene are limited to flight Mach numbers below 6 because of insufficient heat-sink capacity for regenerative engine cooling. Cryogenic fuels such as liquid methane offer both high combustion energy and

large heat-sink capacity. However, above Mach 8 only the ultimate cryogenic fuel, hydrogen, satisfies internal-combustion-engine cooling requirements.

When burned in air, a pound of hydrogen will release 51,000 Btu/lb of fuel burned compared to 18,500 Btu/lb for kerosene. Typically, hydrogen can be heated from the cryogenic storage temperature to as high as 1000°F (800°K) prior to injection and in the process will absorb approximately 5500 Btu/lb, which is a large heat-sink capacity compared with other fuels. This property permits engine components to function at or below allowable temperatures even though the combustion temperature is much greater than the limit for kerosene engines.

The advantages of liquid hydrogen are at least partially offset by the requirement for cryogenic storage and design penalties associated with the low density of the fuel. The effect of the requisite insulated fuel tanks and larger storage volume is greater structural weight and higher drag. The density of hydrogen is roughly one-tenth the density of kerosene, and therefore, the volume assigned to each pound of fuel must be ten times as large for hydrogen as for kerosene. A design requirement of hypersonic aircraft which is a direct result of this need for large tankage volume at conditions where surface temperatures may exceed 2500°R (1400°K) is "minimal surface area per unit volume."

Having concluded that liquid hydrogen is a suitable fuel for hypersonic aircraft, the designer is faced with the responsibility of maximizing the advantages relating to high combustion energy and large heat sink, while minimizing the disadvantages relating to cryogenic storage and low density. The net result is that hydrogen offers substantially better overall aircraft performance than any other fuel at all Mach numbers and, in fact, above Mach 8, it is the only fuel that can meet the requirement for internal-combustion-engine regenerative cooling.

SECTION III
EXTERNAL BURNING

A novel propulsion concept potentially suitable for high-velocity flight is external burning. The general concept may be illustrated by considering a double-wedge aircraft configuration as sketched on the following page.

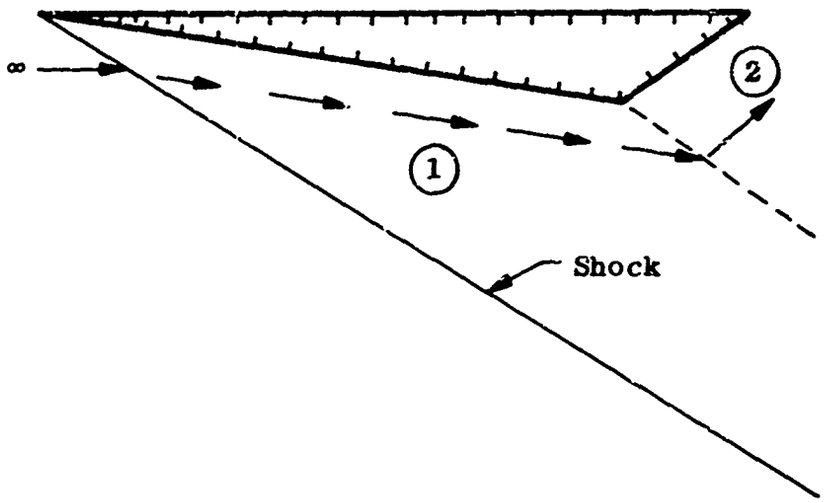

The free stream is compressed by the bow shock, with a resultant pressure rise in region ①. This increased pressure produces lift and contributes to the drag of the vehicle. In the absence of external heat addition, the flow expands at the knee, so that the pressure in the base region, ②, is less than the free-stream pressure. This low base pressure has a detrimental effect on the lift and also contributes to the vehicle drag. The pressure drag per unit frontal area is

$$D_p = p_{①} - p_{②} \tag{30}$$

The object of external heat addition is to effectively compensate for the expansion process between regions ① and ② so that $p_{②} \geq p_{①}$. It is obvious from Eq. (30) that if $p_{②}$ can be maintained at a higher level than $p_{①}$ a net thrust can be obtained.

Propulsion by external heat addition has been studied both experimentally and theoretically by numerous investigations (e.g., Refs. 62, 1970 and 63, 1972). An excellent reveiw of this subject has been compiled by Billig (Ref. 59, 1967). Chushkin (Ref. 64, 1970), in a series of papers since 1968 has given numerical analyses of supersonic nonequilibrium combustion. The numerous analyses postulate either a stationary detonation wave, with planar heat addition, or shock-free constant pressure heat addition. In the following analysis, a constant pressure heat addition scheme will be used in order to make quantitative estimates of the various features. The constant pressure process has been chosen primarily for simplicity. The choice of a shock-force fuel injection process with distributed heat addition rather than a detonative flow model is also supported by the conclusions of Townend et at. (Ref. 58, 1970).

The model used for analysis purposes is shown in the following sketch. Perfect gas relations are assumed to apply and combustion is considered to occur in an ideal manner.

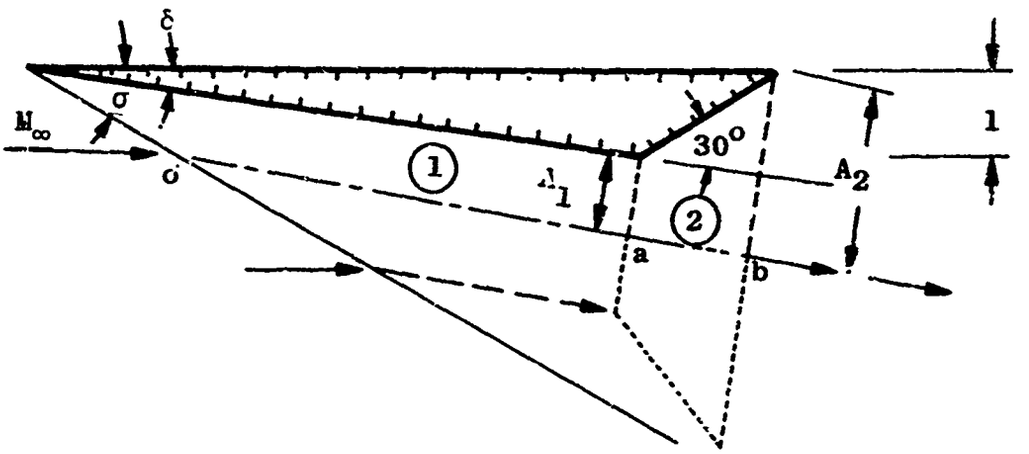

It is assumed that line o-a-b represents the centerline of a nozzle. Region ① has parallel uniform supersonic flow which undergoes a change in area from $2A_1$ at (a) to $2A_2$ at (b). Heat is added in region ② with such a distribution that $p_{①} = p_{②}$, so that uniform pressure is maintained. With this constant pressure assumption, the line a-b represents a "slip plane" and only the region between a-b and the vehicle base requires heat addition.

The necessary relations for numerical analysis can be found from "Influence Coefficients" (Shapiro, Ref. 65, 1953). These are:

$$\frac{dM^2}{M^2} = -2\,\frac{\left(1+\frac{\gamma-1}{2}\,M^2\right)}{1-M^2}\,\frac{dA}{A} + \frac{(1+\gamma M^2)\left(1+\frac{\gamma-1}{2}\,M^2\right)}{1-M^2}\,\frac{dT_o}{T_o} \tag{31}$$

$$\frac{dT}{T} = \frac{(\gamma-1)M^2}{1-M^2}\,\frac{dA}{A} + \frac{(1-\gamma M^2)\left(1+\frac{\gamma-1}{2}\,M^2\right)}{1-M^2}\,\frac{dT_o}{T_o} \tag{32}$$

and

$$\frac{dp}{p} = \frac{\gamma M^2}{1-M^2}\,\frac{dA}{A} - \frac{\gamma M^2\left(1+\frac{\gamma-1}{2}\,M^2\right)}{1-M^2}\,\frac{dT_o}{T_o} \tag{33}$$

For a constant pressure process, these equations become

$$\frac{dA}{A} = \left(1 + \frac{\gamma - 1}{2} M^2\right)\frac{dT_o}{T_o} \tag{34}$$

$$\frac{dT}{T} = \left(1 + \frac{\gamma - 1}{2} M^2\right)\frac{dT_o}{T_o} \tag{35}$$

and

$$\frac{dM^2}{M^2} = \left(1 + \frac{\gamma - 1}{2} M^2\right)\frac{dT_o}{T_o} \tag{36}$$

Therefore,

$$\frac{T_2}{T_1} = \frac{A_2}{A_1} \tag{37}$$

$$\frac{M_2^2}{M_1^2} = \frac{A_1}{A_2} \tag{38}$$

and

$$\frac{T_{o_2}}{T_{o_1}} = \frac{\left(1 + \frac{\gamma - 1}{2} M_2^2\right)}{\left(1 + \frac{\gamma - 1}{2} M_1^2\right)}\frac{M_1^2}{M_2^2} \tag{39}$$

From geometrical considerations, the final area ratio is a function of the initial area, A_1, viz.,

$$\frac{A_2}{A_1} = 1 + \frac{\sin(30°)}{A_1 \sin(30° - \delta)} \tag{40}$$

Since it is desirable that the heat-addition process involve the smallest possible amount of air so that the fuel consumption is kept to a minimum, A_1 should be a minimum. Thus, A_2/A_1 from Eq. (40) should be a maximum, as should T_2/T_1 from Eq. (37). The heat-addition process in region ② reduces the Mach number. One limit on the amount of heat which can be realistically added to the flow is imposed by the requirement that the flow must always be supersonic. Therefore, $M_2 \geq 1$. A second limitation on the amount of heat which can be added to the flow is imposed by the finite heating value of the fuel.

Thus,

$$\Delta T_{o_{max}} = T_{o_2} - T_{o_1} \tag{41}$$

$$= T_2\left(1 + \frac{\gamma - 1}{2} M_2^2\right) - T_1\left(1 + \frac{\gamma - 1}{2} M_1^2\right) \tag{42}$$

and

$$T_{2_{max}} = \Delta T_{o_{max}} - \frac{\gamma - 1}{2} M_2^2 T_2 + T_1\left(1 + \frac{\gamma - 1}{2} M_1^2\right) \tag{43}$$

From Eqs. (37) and (38),

$$M_2^2 T_2 = M_1^2 T_1 \tag{44}$$

Therefore,

$$T_{2_{max}} = \Delta T_{o_{max}} - \frac{\gamma - 1}{2} M_1^2 T_1 + T_1\left(1 + \frac{\gamma - 1}{2} M_1^2\right)$$

$$T_{2_{max}} = \Delta T_{o_{max}} + T_1 \tag{45}$$

For a stcichiometric hydrogen-air mixture,

$$\Delta T_{o_{max}} \approx 6050°(3365°K) \tag{46}$$

The value of T_2 is selected from Eq. (44) with M_2 set equal to unity, with the additional constraint that $T_2 \leq T_{2_{max}}$. That is,

$$T_2 = M_1^2 T_1 \tag{47}$$

unless

$$M_1^2 T_1 > T_{2_{max}}$$

in which case

$$T_2 = T_{2_{max}} \tag{48}$$

Once T_2 is established, M_2 can be found from Eq. (44), A_1 from Eqs. (37) and (40), and finally A_2 is given by Eq. (37) or (38) and A_1. The mass of air to which heat is added is given by

$$\dot{m}_{air} = \rho_1 A_1 V_1 \tag{49}$$

and the total enthalpy change is given by

$$\Delta H = C_p(\bar{T}_{o_2} - T_{o_1})\dot{m}_{\ell} \tag{50}$$

The fuel flow rate is then given by the ratio of the total enthalpy change to the heating value of the fuel. Representative fuel flow rates, pounds of H_2 per second per unit frontal area, are shown in Fig. 26.

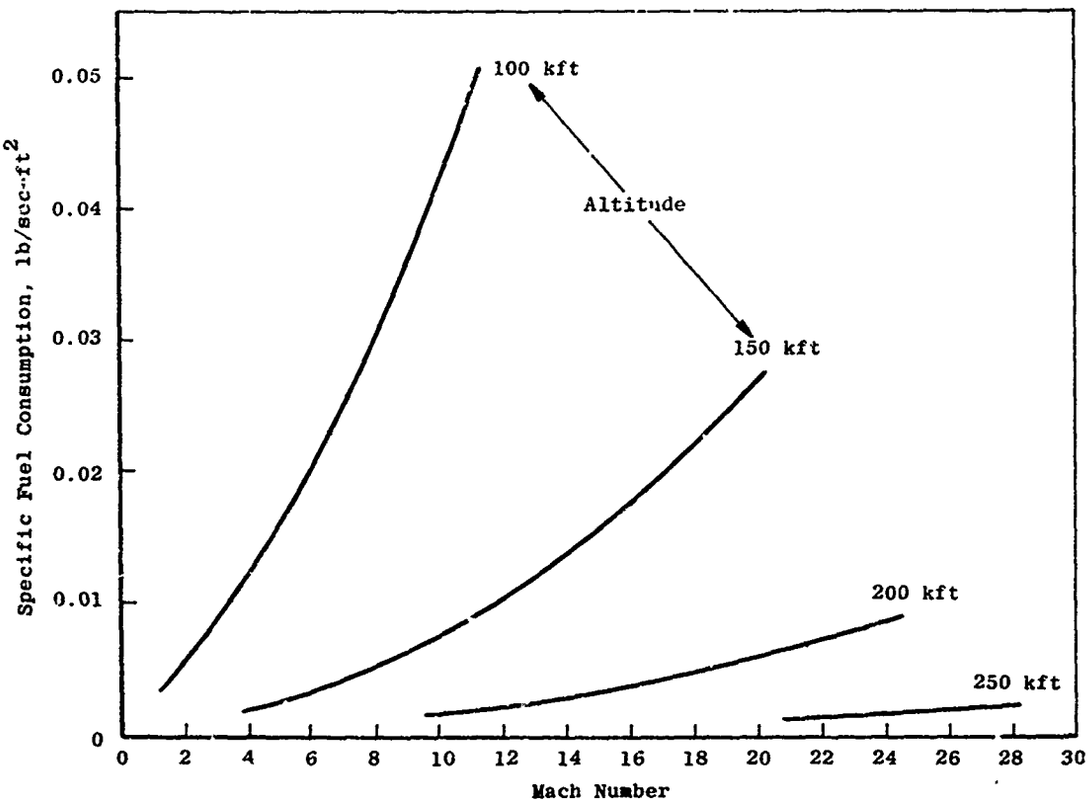

Fig. 26 Specific Fuel Consumption Required to Increase Base Pressure to Forebody Pressure Level

This calculation model is based on perfect-gas flow fields where the shock wave inclination is such that point (a) lies inside the bow shock. Also, this model assumes that an optimum amount of fuel is provided. No information is provided on the thrust available from less than the optimum amount of fuel addition, a case which might arise if the primary use of the fuel is for cooling. Nevertheless, the model does give estimates for the thrust levels, specific impulses, and required fuel flow rates for sustained cruise.

Calculations have been performed for points along the altitude-velocity trajectories shown in Fig. 1, using this analysis model. The inclination of the lower surface is taken equal to be the initial wedge angle.

The first step is to determine the angle of inclination of the lower surface, δ. From Eq. (16) a value of δ may be chosen, i.e., δ for $(L/D)_{max} \approx 1/(Re_{\delta,\ell})^{1/6}$. The initial wedge angle δ has then been taken as

$$\delta \equiv 1/\left(Re_{\delta,\ell}\right)^{1/6} \tag{51}$$

Note that a practical aircraft may require additional volume for payload and fuel, so that $(L/D)_{max}$ may not necessarily be given by Eq. (16). That equation is used here only to obtain some idea of values of δ that may be of interest. Wedge angles for $(L/D)_{max}$ are shown in Fig. 27, assuming a vehicle length of 75 ft. The atmospheric properties are taken from the 1962 Standard Atmosphere, as a function of altitude. These properties, along with the velocity, give a complete description of the free-stream flow.

The bow shock wave inclination, σ, is given implicitly by

$$\sin^2\sigma - \frac{1}{M_\infty{}^2} - \frac{\gamma+1}{2}\,\frac{\tan\delta}{\tan\delta + \cot\sigma} = 0 \tag{52}$$

Once the free-stream properties and the shock wave inclination are found, the properties behind the bow shock in region ① are

$$p_1/p_\infty = \frac{2\gamma M_\infty{}^2 \sin^2\sigma - \gamma + 1}{\gamma + 1} \tag{53}$$

$$M_1{}^2 = \frac{(\gamma-1)(p_1/p_\infty) + (\gamma+1)}{2\gamma(p_1/p_\infty)\sin^2(\sigma-\delta)} \tag{54}$$

and

$$T_1/T_\infty = (p_1/p_\infty)\frac{[(\gamma-1)(p_1/p_\infty) + \gamma + 1]}{[(\gamma+1)(p_1/p_\infty) + \gamma - 1]} \tag{55}$$

And finally the Prandtl-Meyer flow angle is

$$\mu_1 = \sqrt{\frac{\gamma+1}{\gamma-1}}\tan^{-1}\sqrt{\frac{\gamma-1}{\gamma+1}(M_1^2-1)} - \tan^{-1}\sqrt{M_1^2-1} \qquad (56)$$

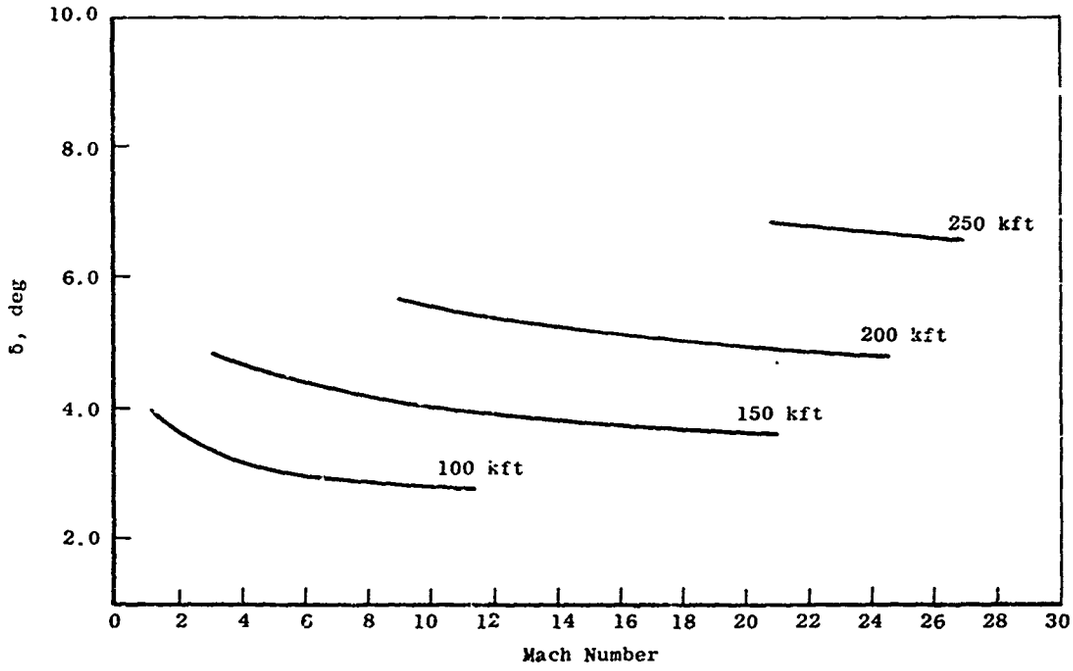

Fig. 27 Angle of Incidence for $(L/D)_{max}$

A calculation of the thrust level provided by external burning requires that the base pressure with burning be compared with the base pressure with no burning. In order to establish the base pressure without burning, the flow is allowed to turn through a Prandtl-Meyer expansion at the knee. The final Mach number is found from

$$\mu_1 + 30° = \sqrt{\frac{\gamma+1}{\gamma-1}}\tan^{-1}\sqrt{\frac{\gamma-1}{\gamma+1}(M_2^2-1)} - \tan^{-1}\sqrt{M_2^2-1} \qquad (57)$$

The base pressure in the absence of heat addition and viscous-flow effects is then obtained from the expressions

$$T_2/T_1 = \frac{\left(1+\frac{\gamma+1}{2}M_1^2\right)}{\left(1+\frac{\gamma+1}{2}M_2^2\right)} \qquad (58)$$

and

$$p_2/p_1 = (T_2/T_1)^{\gamma/(\gamma-1)} \tag{59}$$

The thrust per unit frontal area attributable to external burning is then given by

$$F_t = (p_2 - p_1)_{\text{with burning}} - (p_2 - p_1)_{\text{without burning}}$$

$$= 0 + (p_1 - p_2)_{\text{without burning}} \tag{60}$$

Figure 28 shows the thrust required per unit frontal area from external heat addition as a function of free-stream Mach number for various altitudes. It should be noted that the calculation model used has required that the heat addition be of the correct magnitude to increase the base pressure to that of the pressure in region ①, thereby eliminating the vehicle pressure drag. Therefore, the thrusts available are the thrusts required to overcome pressure drag. The levels obtained are surprisingly small at the higher altitudes. In fact, if one of the trajectories shown in Fig. 1 is traversed, as altitude and velocity increase, the thrust required for sustained cruise actually decreases.

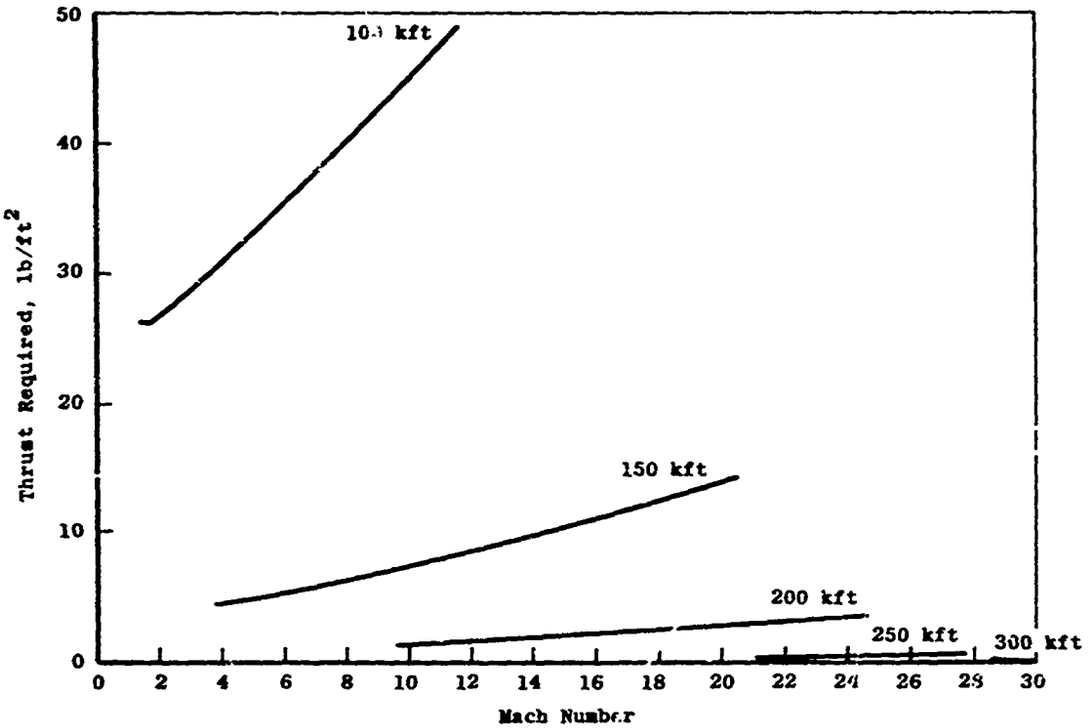

Fig. 28 Thrust Required for Cruise

The ratio of the thrust produced to fuel flow rate gives the specific impulse. Values of this quantity are shown in Fig. 29. Hydrogen fueled rockets have specific impulses on the order of 450 sec. Thus it appears that external burning is superior to rocket power in terms of fuel consumption up to about Mach 20. For a Mach 10 cruise at 200,000 ft, for example, the vehicle range can be increased by a factor of 2 by the use of external burning rather than conventional rocket power.

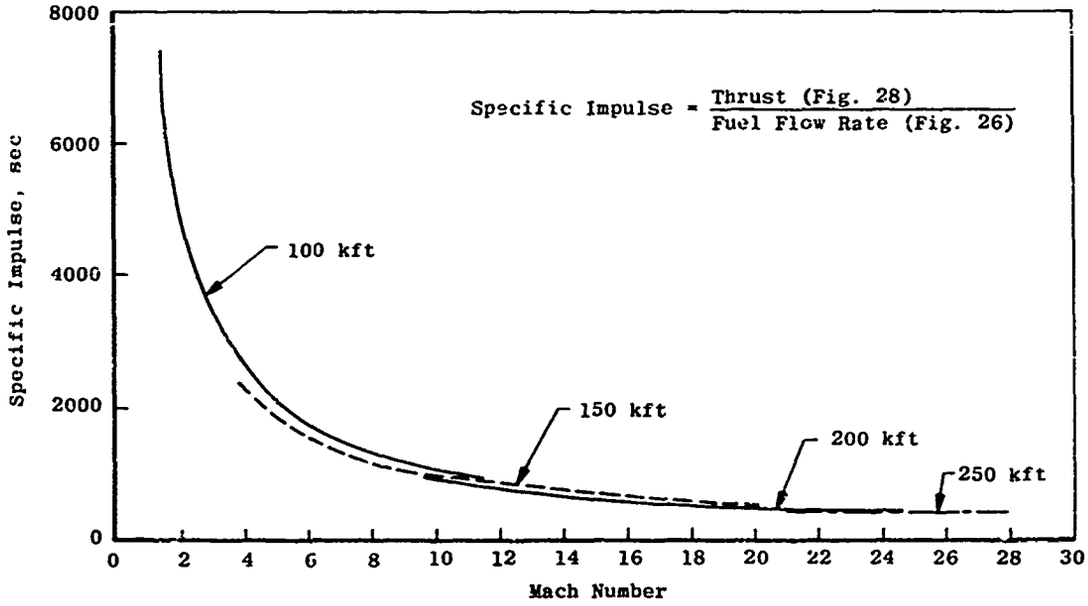

Fig. 29 Specific Impulse

It is obvious that for sustained cruise at high velocities some provision must be made for cooling at least some portions of the vehicle. The use of hydrogen is very attractive for vehicle cooling. An interesting question is whether the fuel required for cooling would also be sufficient for propulsion.

In order to address this question, a new calculation model must be proposed, since in the previous model the thrust was specified and the fuel flow rate was obtained from the calculations. In the present case, the fuel flow rate is dictated by the cooling requirement and the thrust level is unknown. The model used is shown in the sketch on the following page. The flow is allowed to turn through an arbitrary angle β at the knee, so that the area change from ② to ③ and the increase in total temperature are compatible with the amount of heat addition.

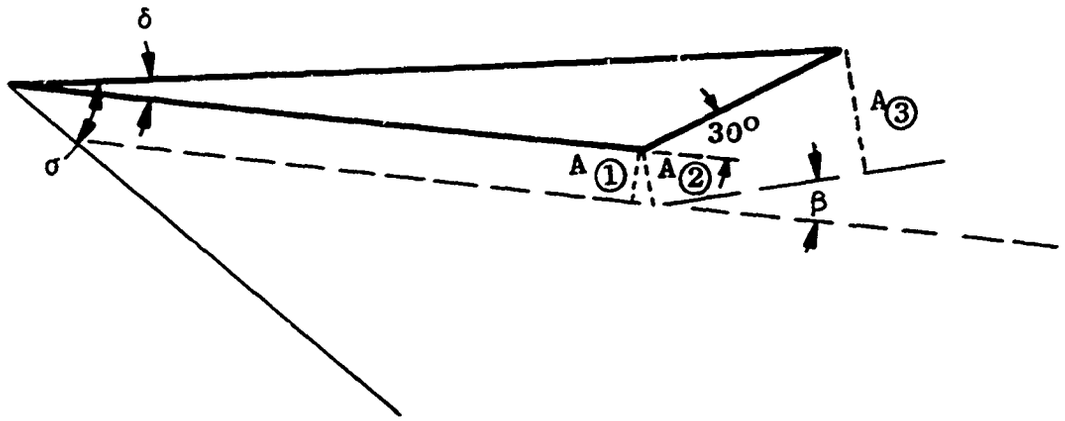

From the geometry in the sketch, the relationship between $A_{①}$, $A_{②}$, and $A_{③}$ is as follows:

$$A_{①} = A_{②}\cos\beta \tag{61}$$

$$A_{③} = A_{②} + \frac{\sin(30^\circ - \beta)}{\sin(30^\circ - \delta)} \tag{62}$$

and

$$A_{③}/A_{②} = 1 + \frac{\cos\beta}{A_{①}} \frac{\sin(30^\circ - \beta)}{\sin(30^\circ - \delta)} \tag{63}$$

From Eqs. (38) and (39) for a constant-pressure heat-addition process between ② and ③,

$$\frac{T_{o_3}}{T_{o_2}} = \frac{\left(A_{③}/A_{②} + \frac{\gamma - 1}{2} M_2^2\right)}{\left(1 + \frac{\gamma - 1}{2} M_2^2\right)} \tag{64}$$

And using Eq. (63), Eq. (64) becomes

$$\frac{T_{o_3}}{T_{o_2}} = \frac{\cos\beta \sin(30^\circ - \beta)}{A_1 \sin(30^\circ - \delta)} \frac{1}{\left(1 + \frac{\gamma - 1}{2} M_2^2\right)} + 1 \tag{65}$$

Multiplying by $T_{O2} A_1$ gives

$$A_1(T_{o_3} - T_{o_2}) = T_{o_1} \cos\beta \frac{\sin(30^\circ - \beta)}{\sin(30^\circ - \delta)} \frac{1}{\left(1 + \frac{\gamma - 1}{2} M_2^2\right)} \tag{66}$$

The amount of heat added to the flow is given by

$$C_p \rho_1 V_1 A_1 (T_{o_3} - T_{o_2}) = h_{H_2} \dot{W}_{H_2} \tag{67}$$

where h_{H_2} is the heating value of hydrogen and $\dot{W}_{H_2}$ is the flow rate. Therefore,

$$\frac{h_{H_2} \dot{W}_{H_2}}{C_p \rho_1 V_1} = T_{o_1} \frac{\cos\beta \sin(30° - \beta)}{\sin(30° - \delta)} \frac{1}{\left(1 + \frac{\gamma - 1}{2} M_2^2\right)} \tag{68}$$

Since both β and M_2 appear in Eq. (68) and both are unknown, an additional relationship between β and M_2 must be used along with Eq. (68) to find M_2 and β. This additional relation is obtained from the Prandtl-Meyer turning angle, viz.,

$$\mu_1 + \beta = \sqrt{\frac{\gamma + 1}{\gamma - 1}} \tan^{-1} \sqrt{\frac{\gamma - 1}{\gamma + 1}(M_2^2 - 1)} - \tan^{-1} \sqrt{M_2^2 - 1} \tag{69}$$

Combining Eqs. (68) and (69), an implicit expression for β may be found, i.e.,

$$\beta = -\mu_1 + \sqrt{\frac{\gamma + 1}{\gamma - 1}} \tan^{-1} \sqrt{\frac{2}{\gamma + 1}\left[\frac{\gamma}{\gamma - 1} \frac{p_\infty V_\infty}{h_{H_2} \dot{W}_{H_2}} \left(1 + \frac{\gamma - 1}{2} M_\infty^2\right) \frac{\sin\sigma \sin(30° - \beta)\cos\beta}{\sin(\sigma - \delta)\sin(30° - \delta)} - \frac{\gamma + 1}{2}\right]}$$

$$- \tan^{-1} \sqrt{\frac{2}{\gamma - 1}\left[\frac{\gamma}{\gamma - 1} \frac{p_\infty V_\infty}{h_{H_2} \dot{W}_{H_2}} \left(1 + \frac{\gamma - 1}{2} M_\infty^2\right) \frac{\sin\sigma \sin(30° - \beta)\cos\beta}{\sin(\sigma - \delta)\sin(30° - \delta)} - \frac{\gamma + 1}{2}\right]} \tag{70}$$

Once β is found from Eq. (70), M_2 can be found from Eq. (69) or (68). The product $A_{①}(T_{o_3} - T_{o_2})$ has been fixed by Eq. (66) or (67). In order to fix $A_{①}$ or $(T_{o_3} - T_{o_2})$, some assumption has to be made about the equivalence ratio. If a stoichiometric mixture is assumed, $A_{①}$ is a minimum and $(T_{o_3} - T_{o_2})$ a maximum. If a leaner mixture is used, $A_{①}$ increases and $(T_{o_3} - T_{o_2})$ decreases appropriately. It appears advantageous to provide the most heating possible to the least amount of air, i.e., stoichiometric mixture. This assumption then fixes $A_{①}$ and, through Eqs. (61) and (62), $A_{②}$ and $A_{③}$.

The method of calculation of the hydrogen flow rate, $\dot{W}_{H_2}$, required for vehicle cooling is given in the next section. These fuel flow rates have been used in the equations developed in this section to determine

the thrust levels which could be obtained, with the fuel flow rate limited to that required for cooling alone.

The results show that, at most, only about one percent of the thrust required to overcome pressure drag can be obtained by burning hydrogen at the rate dictated by cooling requirements. For sustained cruise at a particular cruise condition, additional fuel must be provided. This also indicates that a fuel other than hydrogen might possibly be used, which is a less efficient coolant with no penalty.

SECTION IV
REGENERATIVE COOLING

4.1 DEFINITION OF COOLING REQUIREMENT

The principal cooling requirements are that the vehicle interior thermal environment be suitable for crew (if any) and electronics equipment, and that the outer vehicle skin be locally protected when necessary from destructively high temperatures caused by large heating loads. If the vehicle is designed for sustained cruise in a thermally severe environment, the heat capacity of the basic structure cannot provide sustained heat protection.

The sketch below shows the relationships between the quantities of interest.

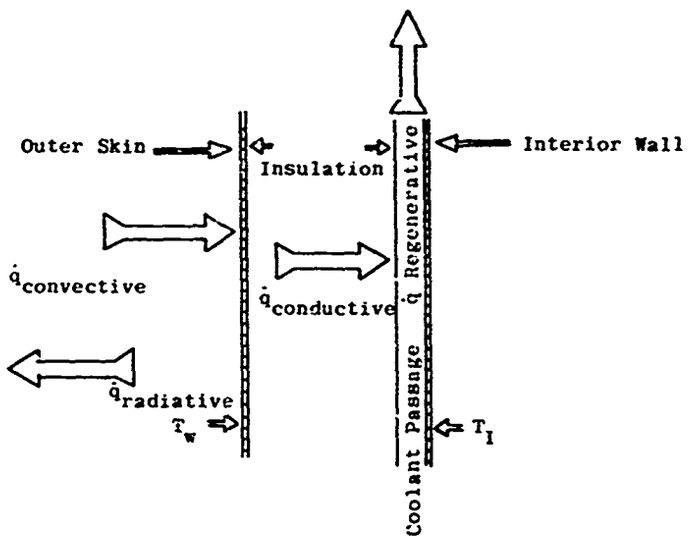

In order to maintain the interior temperature, T_I, at a constant value, $\dot{q}_{conductive} = \dot{q}_{regenerative}$, and from a heat balance, $\dot{q}_{convective} - \dot{q}_{radiative} = \dot{q}_{conductive}$. An upper limit on $\dot{q}_{radiative}$ is imposed by the requirement that the wall temperature, T_w, be less than some maximum value. This, in turn, establishes a minimum value for $\dot{q}_{conductive}$, which may be greater than or equal to zero. Thus, for portions of the vehicle where $\dot{q}_{convective} < \dot{q}_{radiative}$ at $T_{w_{max}}$, no regenerative cooling is required. The extent of the external surface which must be provided with cooling and the amount of cooling required are then governed by $T_{w_{max}}$ and the local $\dot{q}_{convective}$.

4.2 HEAT-TRANSFER ANALYSIS

For the purposes of analysis, it is assumed that the heating load can be approximated by that experienced on the windward side of a flat plate at the angle of attack which gives $(L/D)_{max}$. The leading edge is assumed to be sharp.

The convective heating rate for this case (Griffith et al., Ref. 66, 1970) is

$$\dot{q}_w = 0.352 \rho_\infty U_\infty (h_o - h_w) \sqrt{\frac{\rho_1 U_1 C^*}{\rho_\infty U_\infty Re_{x,\infty}}} \tag{71}$$

where

$$C^* = \frac{\mu^*/T^*}{\mu_\infty/T_\infty} \tag{72}$$

$$Re_{x,\infty} = \frac{\rho_\infty U_\infty x}{\mu_\infty} \tag{73}$$

and

$$h^* = C_p T^* = 0.5(h_1 + h_w) + 0.11\sqrt{P_r}\, U_1^2 \tag{74}$$

The radiative cooling rate is given by

$$\dot{q}_R = \epsilon\sigma(T_w^4 - T_E^4) = \epsilon\sigma T_w^4 \tag{75}$$

From Eq. (71), $\dot{q}_w$ is proportional to $1/\sqrt{x}$ and from Eq. (75), $\dot{q}_R$ is proportional to T_w^4. The following sketch shows the amount and extent of cooling required for an example case:

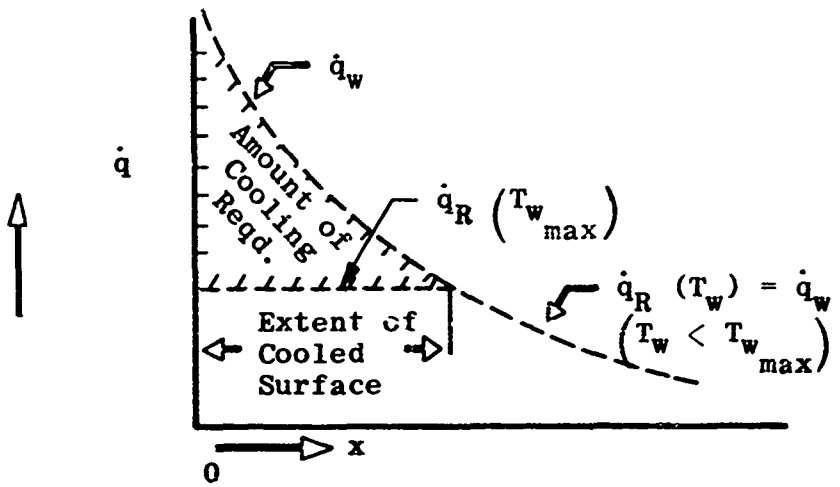

Distance from Leading Edge

From the sketch, the extent of the surface which requires cooling, x_1, can be found by setting $\dot{q}_w(T_{w_{max}}, x_1) = \dot{q}_R(T_{w_{max}})$. Then

$$0.352\rho_\infty U_\infty (h_o - h_{w_{max}}) \sqrt{\frac{p_1 U_1 C^* \mu_\infty}{p_\infty \rho_\infty U_\infty^2 x_1}} = \epsilon\sigma(T_{w_{max}}^4 - T_E^4) \tag{76}$$

Thus,

$$x_1 = \frac{p_1 U_1 C^* \mu_\infty}{R T_\infty} \left\{ \frac{0.352\,(h_o - h_{w_{max}})}{\epsilon\sigma(T_{w_{max}}^4 - T_E^4)} \right\}^2 \tag{77}$$

The heat flux which must be absorbed by the fuel per unit vehicle width is then

$$\overline{\dot{q}_{H_2}} = \int_0^{x_1} \left[\dot{q}_w(T_{w_{max}}) - \dot{q}_R(T_{w_{max}}) \right] dx \tag{78}$$

Define

$$\dot{q}_{w_1} = \dot{q}_w(T_{w_{max}}, x_1) \tag{79}$$

Integration of Eq. (78) then gives

$$\overline{\dot{q}_{H_2}} = (2\dot{q}_{w_1} - \dot{q}_{R_{max}})x_1 \tag{80}$$

The heat storage capacity of H_2 has been taken to be

$$q_{ST} = 5200 \text{ Btu/lb}$$

Finally, the mass flow rate of coolant per unit vehicle width required is given by

$$\dot{W}_{H_2} = \frac{(2\dot{q}_{w_1} - \dot{q}_{R_{max}})x_1}{q_{ST}} \tag{81}$$

The extent of the surface which requires regenerative cooling (Eq. 77) is shown in Fig. 30 for various altitudes as a function of free-stream Mach number. In these calculations, only the optimum wedge angle (Fig. 27) has been considered.

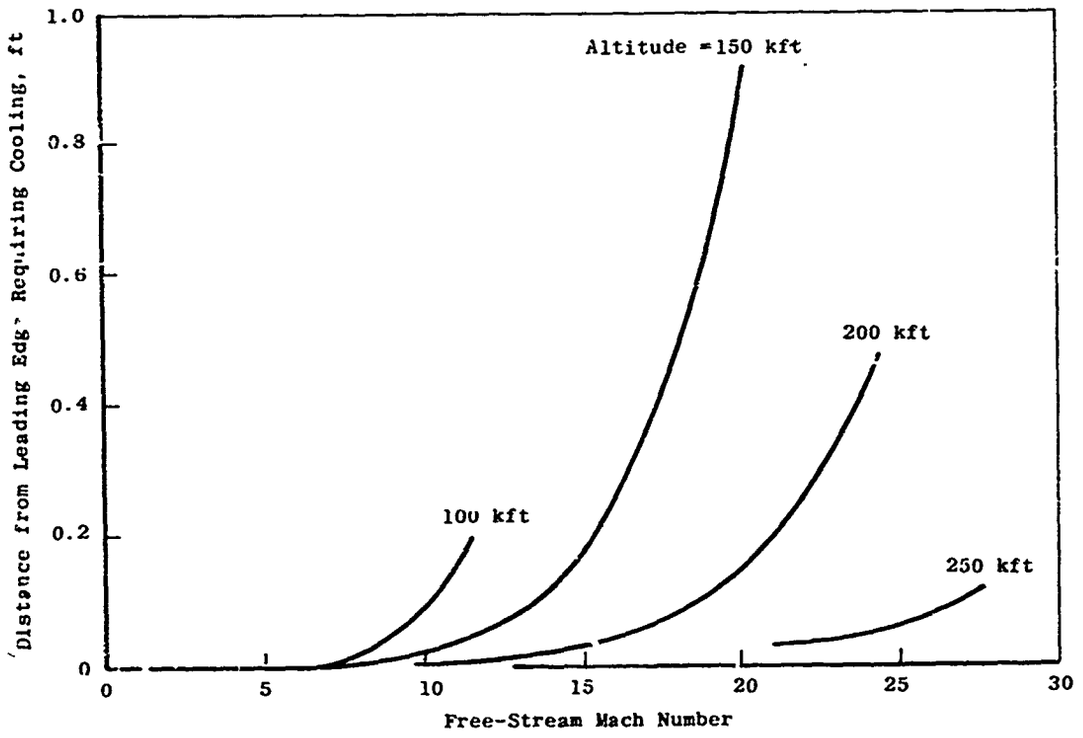

Fig. 30 Extent of Surface Requiring Regenerative Cooling

The required mass flow rate of coolant per unit vehicle width (Eq. 81) is shown in Fig. 31 for various altitudes as a function of Mach number. This may be related to the fuel flow rate per unit frontal area y multiplying by the ratio of the projected frontal area requiring cooling to the frontal area of the vehicle. It is obvious from the results shown in Fig. 31 that the coolant flow rate is very small compared with that required for propulsion, shown in Fig. 26.

It should be emphasized that only the aerodynamic heating on the windward surfaces has been considered. An additional heating load which has not been considered and which may be appreciable is that experienced by the surface exposed to the externally heated flow. No attempt has been made to estimate the magnitude of this heating load.

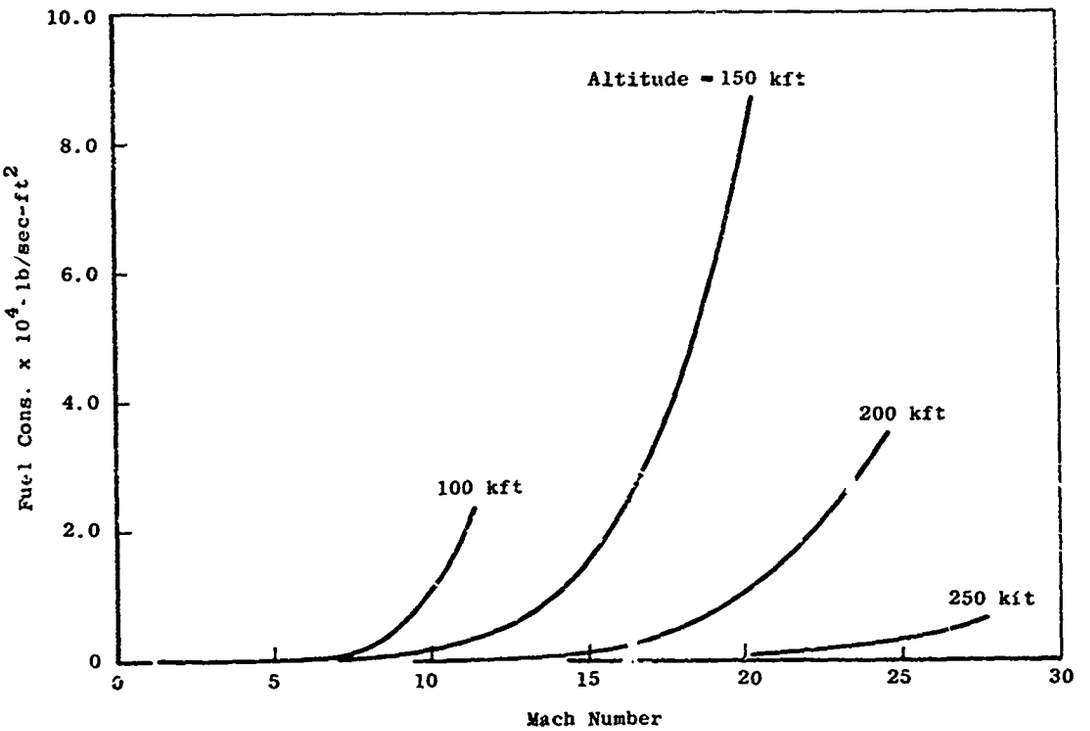

Fig. 31 Specific Fuel Consumption Required for Cooling Windward Aerodynamic Surfaces

SECTION V
CONCLUSIONS

One conclusion is that the fuel required for propulsion by an external-burning configuration may exceed the fuel required for

cooling windward aerodynamic surfaces in the simple example analyzed. This has two important consequences. First, the cooling efficiency of the fuel may be a secondary consideration in the choice of fuel, with the heating value, specific weight and volumetric requirements becoming the primary criteria. Secondly, since an excess cooling capability is available, the possibility remains that vehicle configurations which require additional cooling might be used without undue penalty. Possible configurations include those with multiple compression shocks for improved compression efficiency and waveriders.

In terms of propulsion efficiency, i.e., specific impulse, external or internal burning scramjets offer an advantage over pure rocket propulsion up to about Mach 20. Although this appears to be a large advantage, the small thrusts required for high velocities at high altitudes tend to discount this advantage, especially when the technical difficulties of developing an operational external combustor are weighed against the simplicity of operational throttlable rocket engines.

It is interesting to note that remarks presented by Sedov, Struminskiy, and Cherniy (Ref. 67, 1970) at a session of the Academy of Sciences of the USSR included the following, as translated:

(i) In contemporary and particularly in future vehicles designed for high speeds, the lifting force and thrust will be developed in a single object. In other words, the separation between lift, drag, and thrust will cease to be appropriate.

(ii) In hypersonic flight vehicles the engine will be incorporated in the lifting surface and will basically be derived from the theories of ignition, combustion, and detonation in spatial supersonic flows with shock waves. In designs of hypersonic direct-flow air-reactive engines (GPVRD), the combustion of the mixture of fuel and air takes place immediately behind the shock wave and with the expansion of the combustion products, thrust and lifting forces are developed simultaneously. Future GPVRD designs with combustion in the external flow and in the trail behind the body are also possible. The development of the indicated vehicles must depend upon research on the structure of detonation waves and on the mechanism of mixture formation and combustion; the principal fact of the possibility of self-oscillations has been

established, and this requires further study and control. While earlier engines and vehicles could be considered separately by taking into account their interaction in linear approximations, now they constitute a single system which must be investigated as a whole.

(iii) The above-mentioned and other scientific problems are contained in the coordinated plan of the Scientific Council on the Mechanics of Liquids and Gases; ...

The foregoing, plus other evidence of research in this area of aircraft design, suggests that external-burning, lifting-body vehicles may appear in the future. Although the technical problems are not insignificant, there do not seem to be any which are beyond early solution if a need for such a vehicle were established. Its airplane like qualities would make it particularly suitable for applications requiring relatively long duration, highly maneuverable flight characteristics.

REFERENCES

1. Nesterenko, G. "Between the Stratosphere and Space. 1. Hypersonic Aircraft and Engines." AD691670 (FTD-MT-24-57-69) Translation of Kryl'ya Rodiny, Vol. 19, No. 9, 1968, pp. 26-27.

2. McCauley, W. D., Editor. "Proceedings of Boundary Layer Transition Specialists Workshop." Aerospace Corporation, San Bernardino, California, December 20, 1971.

3. Hankey, W. L. and Elliott, G. A. "Hypersonic Lifting Body Optimization." Journal of Spacecraft and Rockets, Vol. 5, No. 12, December 1968, pp. 1463-1467.

4. Becker, John V. "Studies of High Lift/Drag Ratio Hypersonic Configurations." Proceedings of the 4th Congress of the International Council of Aeronautical Sciences, August 24-28, 1964, Spartan Books, Inc., Washington, D. C., 1965, pp. 877-910.

5. Roe, P. L. "Aerodynamics at Moderate Hypersonic Mach Numbers, Optimum Shapes." In "Aerodynamic Problems of Hypersonic Vehicles," von Kármán Institute for Fluid Dynamics, Von Kármán Institute Lecture Series No. 18, 1970.

6. Küchemann, D. "Hypersonic Aircraft and their Aerodynamic Problems." Progress in Aeronautical Sciences (Pergamon Press), Vol. 6, 1965, p. 271-353.

7. Luxton, R. E. and Young, A. D. "Generalized Methods for the Calculation of the Laminar Compressible Boundary-Layer Characteristics with Heat Transfer and Non-Uniform Pressure Distribution." British ARC R&M 3233, 1960.

8. Whalen, R. J. "Viscous and Inviscid Nonequilibrium Gas Flows." Journal of the Aerospace Sciences, Vol. 29, October 1962, pp. 1222-1237.

9. Inger, G. R. "Similitude of Hypersonic Flows over Slender Bodies in Nonequilibrium Dissociated Gases." AIAA Journal, Vol. 1, January 1963, pp. 46-53.

10. Wittliff, C. E. and Sundaram, T. R. "A Study of Hypervelocity Slender Body Flows and Similitudes Including the Effects of Nonequilibrium and Nose Bluntness." AIAA 6th Aerospace Sciences Meeting, New York, Paper 68-14, 1968. (Jan. 22-24)

11. Norman, W. S. "Effect of Real Gas Properties on the Base Pressure of a Blunt-Nosed Vehicle." AIAA Journal, Vol. 7, December 1969, pp. 2347-2349.

12. Edney, B. E. "Effects of Shock Impingement on the Heat Transfer around Blunt Bodies." AIAA Journal, Vol. 6, January 1968, pp. 15-21.

13. Bird, G. A. "Some Methods of Evaluating Imperfect Gas Effects in Aerodynamic Problems." British ARC C.P. No. 397 (Also T.N. Aero 2488, Jan. 1957), 1958.

14. Zienkiewicz, H. K. "Flow about Cones at Very High Speeds." Aeronautical Quarterly, Vol. 8, November 1957, pp. 384-394.

15. Feldman, S. "Hypersonic Conical Shocks for Dissociated Air in Thermodynamic Equilibrium." Jet Propulsion, Vol. 27, December 1957, pp. 1253-1255.

16. Romig, M. F. "Application of the Hypersonic Similarity Rule to Conical Flow of Dissociated Air." Aero/Space Engineering, V. 18, March 1959, pp. 56-59.

17. Nonweiler, T. "Delta Wings of Shapes Amenable to Exact Shock-Wave Theory." Journal of the Royal Aeronautical Society, Vol. 67, Jan. 1963, p. 39-40.

18. Pike, J. "On Lifting Surfaces Supporting One or More Plane Shock Waves." British RAE R&M 3623, 1970.

19. Roe, P. L., Davies, L., and Squire, L. C. "Report on Papers at Euromech 20 on the Aerodynamics of Lifting Bodies at High Supersonic Speeds." British RAE TR-71054, 1971.

20. Squire, L. C. "A Comparison of the Lift of Flat Delta Wings and Waveriders at High Angles of Incidence and High Mach Number. "British A.R.C. 32,555, Hyp. 844, December 1970.

21. Maikapar, G. I. "Wing Shape Selection for Hypersonic Speeds." Izv. AN SSSR. Mekhanika Zhidkosti i Gaza, Vol. 2, No. 4, 1967, pp. 40-49. (Translation: Fluid Dynamics, V. 2, No. 4, July-August 1967, pp. 25-31.)

22. Townend, L. H. "Some Design Aspects of Space Shuttle Orbiters." RAE TR-70139, 1970.

23. Boylan, D. E. and Potter, J. L. "Aerodynamics of Typical Lifting Bodies under Conditions Simulating Very High Altitudes." AIAA Journal, Vol. 5, February 1967, pp. 226-232.

24. Korkegi, R. H. "Survey of Viscous Interactions Associated with High Mach Number Flight." AIAA Journal, Vol. 9, May 1971, pp. 771-784.

25. Hidalgo, Henry and Vaglio-Laurin, Roberto. "High Altitude Aerodynamics and Its Effects on Lifting Reentry Performance." International Astronautical Federation, International Astronautical Congress, 18th, Belgrade, Yugoslavia, Sept. 24-30, 1967, Proceedings. Vol. 3: Propulsion and Reentry. Edited by M. Lunc. Oxford, Pergamon Press, Ltd., 1968, pp. 231-245.

26. Koppenwallner, G. "Wind Tunnel Testing on Real Configurations in Hypersonic Flow. A Summary of Current Studies at the DFVLR." In "High Altitude Aspects of Lifting Reentry Vehicles," von Kármán Institute for Fluid Dynamics, von Kármán Institute Lecture Series No. 38, 1971.

27. Jones, J. G. "The Design of Compression Surfaces for High Supersonic Speeds Using Conical Flow Fields." British RAE Report Aero 2674, ARC 24846, 1963.

28. Pike, J. "On Conical Waveriders." British RAE TR-70090, 1970.

29. Keldysh, V. V. "The L/D Ratio of a Winged Conical Sector under Conditions Corresponding to Sections of the Flow in the Vicinity of a Circular Cone at Zero Angle of Attack." Izv. AN SSSR Mekhanika Zhidkosti i Gaza, Vol. 3, No. 6, 1968, pp. 118-121. Translation: Fluid Dynamics, Vol. 3, No. 6, Nov.-Dec. 1968, pp. 81-83.

30. Maikapar, G. I. "A Wing with the Maximum Lift/Drag Ratio at Supersonic Velocity." PMM, Vol. 30, No. 1, 1966, pp. 186-189.

31. Keldysh, V. V. and Maikapar, G. I. "Gasdynamic Design Considerations for Hypersonic Aircraft." Izv. AN SSSR Mekhanika Zhidkosti i Gaza, No. 3, May-June 1969, pp. 177-185. (In Russian)

32. Gonor, A. L. "On Three-Dimensional Bodies of Minimum Drag at High Supersonic Speeds." Prikladnaya Matematika: Mekhanika, Vol. 27, No. 1, 1963, pp. 185-189. Translation: PMM: Journal of Applied Mathematics and Mechanics, Vol. 27, 1963, pp. 273-285.

33. Gonor, A. L. "Exact Solution of the Problem of Supersonic Flow of Gas Past Some Three-Dimensional Bodies." Prikladnaya Matematika: Mekhanika, Vol. 28, No. 5, 1964, pp. 974-976. Translation PMM: Journal of Applied Mathematics and Mechanics, Vol. 28, No. 5, pp. 1178-1180.

34. Gonor, A. L. "Determination of the Shape of a Three-Dimensional Optimum Body Taking Friction Forces into Account." Akademiia Nauk, SSSR, Izuestiia, Mekhanika, No. 4, July-August 1965, pp. 24-30.

35. Gonor, A. L. "Certain Three-Dimensional Flows with Mach Interaction of Shock Waves." AN SSSR. Izvestiya Mekhanika Zhidkosti i Gaza, Vol. 1, No. 6, 1966, pp. 135-140. Translation: Fluid Dynamics, Vol. 1, No. 6, Nov.-Dec. 1966, pp. 87-90.

36. Gonor, A. L. "Optimum Shapes of Bodies in Hypersonic Gas Flow." Proceedings of the 6th Congress of the International Council of the Aeronautical Sciences, Munich, Germany, Sept. 9-13, 1968, Paper No. 68-19

37. Gonor, A. L., Kazakov, M. N., and Schvets, A. I. "Experimental Investigation of the Drag of Some Bodies in a Hypersonic Flow." (Sb. Z-y Vses. s"yezd po teor. i prikl. Mekhan., Annota-dokl. M.) 1968, p. 100.

38. Hankey, W. L. "Some Design Aspects of Hypersonic Vehicles." U.S.A.F. ARL 70-0049, 1970.

39. Keldysh, V. V. and Maikapar, G. I. "Aerodynamics and Heat Transfer of Waveriders." Proceedings, 7th Congress of the International Council of the Aeronautical Sciences, Paper No. 70-18, Rome, Italy, Sept. 14-18, 1970.

40. Maikapar, G. I. "Aerodynamic Heating of Lifting Bodies." International Astronautical Federation, Congress, 19th, New York, New York, Oct. 13-19, 1968, Proceedings, Vol. 3: Propulsion Re-Entry Physics. Lunc, M., editor. Oxford, Pergamon Press, 1970, pp. 325-335.

41. Eggers, Jr., A. J., Petersen, R. H., and Cohen, N. B. "Hypersonic Aircraft Technology and Applications." Astronautics and Aeronautics, Vol. 8, No. 6, June, 1970, pp. 30-41.

42. Henry, J. R. and McLellan, C. H. "Air-Breathing Launch Vehicle for Earth-Orbit Shuttle - New Technology and Development Approach." Journal of Aircraft, Vol. 8, No. 5, May 1971, pp. 371-387.

43. Townend, L. H. "Ramjet Propulsion for Hypersonic Aircraft." British RAE Tech. Memo Aero 917, 1966.

44. Small, W. J., Kirkham, F. S., and Fetterman, D. E. "Aerodynamic Characteristics of a Hypersonic Transport Configuration at Mach 6.86." NASA TN D-5885, 1970.

45. Neumann, R. D. "Special Topics in Hypersonic Flow." In "Aerodynamic Problems of Hypersonic Velocities," von Kármán Institute for Fluid Dynamics, von Kármán Institute Lecture Series 18, 1970.

46. Ceresuela, R. "Hypersonic Vehicles Propulsion, Part IV – Aerodynamic Problems." In "Aerodynamic Problems of Hypersonic Vehicles," von Kármán Institute for Fluid Dynamics, von Kármán Institute Lecture Series 18, 1970.

47. Whitehead, A. H. "Effect of Vortices on Delta Wing Lee-Side Heating at Mach 6." AIAA Journal, Vol. 8, March 1970, pp. 599-600.

48. Rao, D. M. "Shock Interaction Effect on a Flapped Delta Wing at M = 8.2." AIAA Journal, Vol. 9, May 1971, pp. 965-986.

49. Whitehead, Jr., A. H. and Bertram, M. H. "Alleviations of Vortex-Induced Heating to the Lee Side of Slender Wings in Hypersonic Flow." AIAA Journal, Vol. 9, n. 9, Sept. 1971, pp. 1870-72.

50. Cubbage, J. M. and Kirkham, F. S. "Investigation of Engine-Exhaust-Airframe Interference on a Cruise Vehicle at Mach 6." NASA TN D-6060, 1971.

51. McGhee, R. J. "Jet-Plume-Induced Flow Separation on a Lifting Entry Body at Mach Numbers from 4.00 to 6.00." NASA TM X-1997, 1970.

52. Fong, M. C. "An Analysis of Plume-Induced Boundary-Layer Separation." Journal of Spacecraft and Rockets, Vol. 8, No. 11, Nov. 1971, pp. 1107-1113.

53. Boger, R. C., Rosenbaum, H., and Reeves, B. L. "Flow Field Interaction Induced by Underexpanded Exhaust Plumes." AIAA Paper 71-562, AIAA Fluid and Plasma Dynamics Conference, 4th, Palo Alto, Calif., June 21-23, 1971. (To be published in AIAA Journal).

54. Hartunian, R. A. and Spencer, D. J. "Experimental Results for Massive Blowing Studies." AIAA Journal, Vol. 5, Aug. 1967, pp. 1397-1401.

55. Kubota, T. and Fernandez, F. L. "Boundary-Layer Flows with Large Injection and Heat Transfer." AIAA Journal, Vol. 6, January 1968, pp. 22-28.

56. Pappas, C. C. and Lee, G. "Heat Transfer and Pressure on a Hypersonic Blunt Cone with Mass Addition." AIAA Journal, Vol. 8, May 1970, pp. 954-956.

57. Marvin, J. G. and Akin, C. M. "Combined Effects of Mass Addition and Nose Bluntness on Boundary-Layer Transition." AIAA Journal, Vol. 8, May 1970, pp. 857-863.

58. Townend, L. H., Holbeche, T. A., Cox, S. G., and Pratt, N. H. "Analysis of External Combustion on Lifting-Propulsive Bodies, and Shock Tunnel Tests at $M_\infty \simeq 7$ and 10." British RAE TR 70060, 1970.

59. Billig, F. S. "External Burning in Supersonic Streams." Johns Hopkins University TM TG-912, 1967.

60. Kallergis, M. "Investigation of External Supersonic Combustion." British RAE Library Translation 1453 (From German Document DGLR-26), 1969.

61. Quick, A. W. "Several New Research Results in the Fields of Flow with Energy Supply." AIAA Journal, Vol. 7, Aug. 1969, pp. 1410-1420.

62. Maurer, F., Niezgodka, J., and Post, H. "Experimental Studies of Heat Addition in the Supersonic Flow Field around Bodies of Revolution on a Flat Plate in Shear Flow." Translated by L. Holtschlag from German Aeronautics and Astronautics Research Report 70-64, December 1970.

63. Maurer, F. "Heat Addition in Supersonic Flow by Means of Hydrogen Combustion on a Flat Plate in Tangential Flow." German Aeronautics and Astronautics Research Report 70-64, (JHU Trans. 2624), March 1972.

64. Chushkin, P. I. "Numerical Analysis of Combustion in Supersonic Flows." Computing Center of the USSR Academy of Sciences, Moscow. 7th Congress of the International Council of the Aeronautical Sciences, Rome, Italy, Paper No. 70-52, 1970.

65. Shapiro, A. H. The Dynamics and Thermodynamics of Compressible Fluid Flow. Vol. 1, 1953, The Ronald Press Co., New York, pp. 231.

66. Griffith, B. J., Norman, W. S., and Boylan, D. E. "Hypersonic Heat-Transfer Rates on an AFFDL 80-deg Slightly Blunted Delta Wing." AEDC-TR-70-178 (AD876317), October 1970.

67. Sedov, L. I., Struminskiy, V. V., and Cherniy, G. G. "Modern Problems in the Mechanics of Liquids and Gases." Presented at Jubilee Scientific Session of the General Assembly of the Division of Mechanics and Control Processes of the USSR Academy of Sciences in Honor of V.I. Lenin's 100th Birthday. 1970.